PLASMA RESEARCH

CASE INSTITUTE OF TECHNOLOGY

UNIVERSITY CIRCLE • CLEVELAND 6, OHIO

AN EXPERIMENTAL STUDY OF THE RELATIONSHIP BETWEEN MOVING STRIATIONS AND PLASMA-ACOUSTIC WAVES

NSG-198

by

D. A. Meskan

Technical Report A-40

Supported in part by the National Aeronautics and Space Administration.

ABSTRACT

The velocity, attenuation, and frequency of moving striations in the positive column of a hot cathode glow discharge are determined experimentally. Plasma-acoustic wave dispersion relations which would be appropriate for explaining these striations by means of a linear fluid model are derived. The properties of various large amplitude waves predicted by nonlinear fluid models are discussed. A comparison of the striations' behavior and the plasma-acoustic wave theories demonstrates that the frequently assumed relationship between these two phenomena does not exist.

The experiments were performed in an argon discharge at pressures from 20 to 480 mtorr. and with discharge current densities on the order of 25 ma/cm^2. Typical electron densities and temperatures were 2 x 10^{10}cm^{-3} and 2 x 10^4 °K. The velocity of the striations varied from 2.1 x 10^5 to 1.3 x 10^4 cm/sec., while the frequency varied from 6 x 10^2 to 2.3 x 10^4 cycles per second.

ACKNOWLEDGMENTS

The author gratefully acknowledges and thanks Professor B. Samuel Tanenbaum for his many contributions to this investigation, and Professor Robert E. Collin for his advice and good counsel.

The construction of various pieces of equipment by Messrs. Byron Watson, Imre Szilagyi, and Edward Parillo, is very much appreciated, as is Miss Jeanette Yount's preparation of the manuscript.

The financial support was provided by the National Aeronautics and Space Administration.

TABLE OF CONTENTS

LIST OF TABLES

LIST OF ILLUSTRATIONS

CHAPTER I

INTRODUCTION

Striations - alternate regions of increased and diminished light intensity in the positive column of low pressure gaseous discharges--were seen as early as 1843. Although the experiments of many investigators since that time have contributed to the qualitative understanding of this phenomenon, only a relatively modest amount of significant quantitative data has been accumulated. With one recent exception, attempts to explain the origin and propagation of the striations theoretically have met with extremely limited success. The core of the problem has always been the difficulty in devising a theory which is uncomplicated enough to compare with experimental work and yet contains all of the pertinent parameters of a gaseous discharge. Despite these inherent difficulties, the field continues to attract many plasma physicists.

It is the purpose of this paper to present the results of observations made on self-propagating disturbances in a gas discharge tube operating at pressures between .02 and .5 torr., a range of pressure one to two orders of magnitude lower than that used for most previously reported striation experiments.

We will first show that at these lower pressures the striations behave similarly to those observed at higher pressures, and then demonstrate that neither a linear nor a non-linear theory of plasma-acoustic waves can adequately describe the propagation of the striations.

A brief survey will first be made of previous experimental and theoretical results with emphasis on work related to striations of the type which move through the positive column from the anode toward the cathode.

One of the most persistent theories relates the striations to the longitudinal ion waves which were described by Tonks and Langmuir in 1929.[8,7,14] According to this explanation, the bright regions of the discharge correspond to density maximums in a propagating wave, or nodes in a standing wave. The standing wave would be composed of a wave traveling from anode to cathode, plus a wave reflected from the negative end of the positive column. Appropriate phase shift upon reflection could cause the nodes to travel away from the anode. Fowler suggested that this type of wave could grow in a non-linear fashion and become a shock wave of "moderate strength", the striations then appearing at the position of the shock front.[2] If the ion wave interpretation is correct, then the wave could be initiated by

instabilities in the column or at its boundaries.

Another approach using a wave model is that of Robertson[4] and Oleson and Watanabe.[5] Using a theory in which the ionization and excitation processes are explicitly included in the initial equations, they find that wave-like solutions are possible. The parameters of these theories are very complicated, and usable dispersion relations can only be found for the most simplified cases. This type of wave could be generated spontaneously in the positive column since it is intimately related to the physical processes responsible for maintaining the discharge.

Other explanations require the striations to originate at the cathode, anode, and/or Faraday dark space.[1,3] None of these explanations provide a mathematical description of how the disturbance would travel through the positive column, but they each appear to be qualitatively consistent with at least one series of experiments.

The most recent mathematical theory of striations, that of Pekarek,[6] seems to agree quite well with experiments made under particular conditions. At pressures on the order of 1 torr. and higher, a discharge can be made free of striations by passing a current through it which is above the "critical"current. Pekarek finds that applying an impulse disturbance to

such a plasma creates "waves of stratification" which move toward the anode with a phase velocity considerably greater than the striation velocity. The striation then appears as a wave packet composed of waves of stratification. Because the group velocity of the wave packet is directed opposite to the phase velocity of the stratification waves the packet moves away from the anode. The basic physical mechanism here is the propagation of a wave of ionization through the plasma, locally enhancing the plasma density and changing the local electric field strength. It is interesting to note that this theory is a linear theory, and can only be demonstrated experimentally when the conditions are such as to prevent non-linear behavior, i.e., operation with currents greater than the critical current.

Two of the most frequently referenced post-1945 experiments are those of Emeleus, Armstrong, and Neill,[7] and Donahue and Dieke.[1] The experiment of Emeleus et.al. was one of the few where the pressure was below 1 torr. Using a hot cathode mercury vapor discharge at a pressure of 10^{-3} torr., they observed moving striations by means of a wire grid and probes placed in the plasma. Their results were mainly qualitative but it is evident that they considered the striations to be related to longitudinal ion waves. The observation of large amplitudes with no apparent attenuation over the length of the tube caused them

to question whether a linear theory could accurately describe the striations. They also tried to excite ion waves by applying a square wave voltage to the grid in the plasma. No waves were detected and they concluded that their system could not have detected waves of small amplitude because of the large amplitude noise which was present.

Donahue and Dieke's most complete set of data was obtained from an argon discharge at a pressure of 12 torr. A photomultiplier tube monitored the light intensity at a point in the discharge, and the output of the P.M. tube was displayed on an oscilloscope. Although the a-c component of the current in the external circuit was small compared to the total current through the discharge, the photomultiplier showed that the light intensity of the discharge was being modulated by as much as 100%. It was found that several modes of oscillation were possible for a given pressure, and that these modes were determined by conditions within the discharge tube. While in a given mode, a decrease in current caused non-linear increases in the voltage across the tube and in the frequency of the striations. They did not derive an algebraic relationship between voltage or frequency and current. Striations were also found moving from the negative glow to the anode. These "negative" striations had velocities on the order of 10^5 cm/sec., while the

velocity of the "positive" striations varied between 3×10^3 cm/sec. and 3.5×10^4 cm/sec. As a negative striation passed through a positive striation, both slowed down and produced a region of enhanced light intensity. The velocities and positions of striations under various conditions were shown graphically, but were not woven into a general quantitative theory.

After using smear photography to observe striations with velocities on the order of 10^4 cm/sec. and frequencies of a few kilocycles/sec. in neon at 4 torr., Emeleus, Coulter and Cooper[9] reported that their photographs suggested a non-linear wave traveling from the anode and being reflected at the negative end of the positive column; however, no quantitative analysis was given.

Coulter[10] later used smear photography to observe similar striations in a cold cathode neon discharge at pressures from 2 to 60 torr. His results indicated that for this range of pressures the striation velocity was given by $V = \text{const.}\ p^{-1/2}$. It was also stated that the velocity was rather insensitive to the magnitude of the current, although the data indicated a trend for the velocity to increase as the current was increased; the trend becoming more pronounced as the pressure was reduced.

Negative striations were observed only near the Faraday dark space.

An increase in the electron density in the striation was measured by Sodomsky, using microwave techniques.[11] In a neon discharge at a pressure of 0.5 torr., he found that the region between striations had an electron density on the order of 10^{10} cm^{-3}, while in the striation the density was about five times greater. The light intensity was greatest at the cathode side of the high density region. The velocity of the striations was on the order of 10^5 cm/sec.

The approximate operating conditions for the preceeding experiments are summarized in Figure (1-1), and their main features can be summarized as follows:

1. Coulter finds that the velocity of the striations in neon is given by $V = \text{Const.}\ p^{-1/2}$.
2. Striations in the rare gases are usually seen to travel away from the anode.
3. Although the velocity of the striations is not sensitive to the discharge current, a trend for the velocity to increase with increasing current is seen as the pressure is reduced.
4. For a given pressure, and a given mode of oscillation, the frequency of oscillation increases

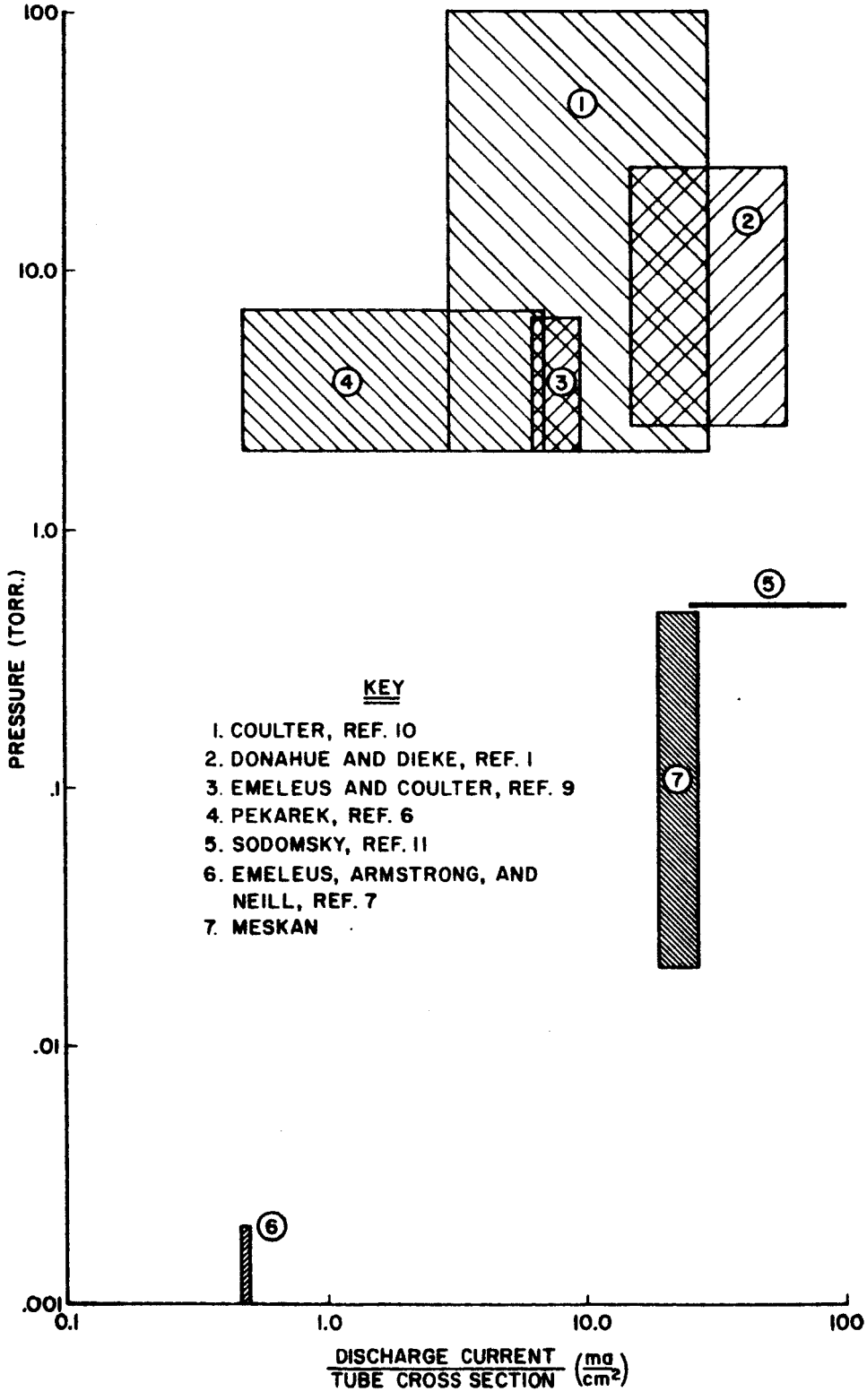

FIG. 1-1 OPERATING RANGES OF VARIOUS EXPERIMENTS.

non-linearly with decreasing discharge current.

5. The light intensity can be strongly modulated, even if the current variations are small.
6. The velocity and frequency are determined principally by conditions inside the discharge tube.

Many more references to experiments and theory can be found in the article by Francis in Reference (12), and the review article by Emeleus in Reference (13).

Chapter 2 of this paper discusses the theories of plasma-acoustic wave propagation which we will compare to experimental results. In Chapter 3 the experimental equipment and its operation are described. Chapter 4 contains a description of specific measurements and the results of these measurements. The comparison between these results and the theories of Chapter 2 are made in Chapter 5. Chapter 6 summarizes the conclusions of this paper and suggests future work.

CHAPTER II

THE THEORIES OF LINEAR PLASMA WAVES, FINITE SOUND WAVES, AND SHOCK WAVES

2.1 Introduction

Since the purpose of this paper is to examine the question of whether moving striations can be explained in terms of plasma-acoustic waves, we will first consider the requirements of specific linear and non-linear wave theories which will be of use to us in subsequent chapters. It is appropriate for us to consider a linear theory for this reason; although various investigators, (usually upon observing large amplitude variations of discharge tube parameters in the presence of striations), have questioned the applicability of linear theory, it seems that a systematic attempt to reconcile striation experiments to linear plasma wave theory has not appeared in the literature. Furthermore, it will be shown later in this paper that one of the most obvious discrepancies between the behavior of experimentally observed striations and linear theory is not resolved by the adoption of a non-linear theory.

Details of the linear theory discussed in this chapter are presented in the Appendix.

2.2 Linear Plasma-Acoustic Waves from the Three-Fluid Model

It has been shown by Tanenbaum and Meskan (Reference 19) that for a partly ionized gas whose particle densities and temperatures lie in the ranges

2-1) $10^{10} < N_n < 10^{16}$ cm^{-3}

2-2) $10^{9} < N_{e,i} < 10^{14}$ cm^{-3}

2-3) $T_{i,n} < 10^{4}$°K

2-4) $10^{4} < T_e < 10^{6}$ °K; $T_e < 25\, T_i$,

(where the subscripts e, i, n denote electrons, ions, and neutral atoms) the dispersion relation for the propagation of the longitudinal plane plasma wave known as the ion-acoustic wave is given by

$$2\text{-}5)\quad \frac{k^2 U_e^2}{\omega^2} = \frac{1 - \frac{\omega_e^2}{\omega^2} + i\left(\frac{\nu_e}{\omega} - \frac{\nu' \omega_e^2}{\omega^3}\right)}{1 - \frac{\omega_i^2}{\omega^2} + i\left(\frac{\nu_i + \nu_n}{\omega} - \frac{\omega_i^2 \nu_n}{\omega^3}\right)} .$$

In this paper we will consider ω to be a real quantity and k a complex quantity. The phase velocity is then given by $V_{PH} = \frac{\omega}{\mathrm{Re}\ k}$ and the attenuation factor by $\alpha = \mathrm{Im}\ k$. Letting the subscripts α, β, δ, refer to particles of the α, β, δ kind, the quantities in equation (2-5) are defined as follows:

2-6) $\omega_\alpha^2 = \frac{N_\alpha e^2}{m_\alpha \varepsilon_o}$ plasma frequency (for a singly ionized gas)

2-7) $\nu_{\alpha\beta}$ effective collision frequency for momentum transfer between α and β particles ($\alpha \neq \beta$)

2-8) $\nu_\alpha = \nu_{\alpha\beta} + \nu_{\alpha\delta}$; $\beta, \delta \neq \alpha$; $\beta \neq \delta$

2-9) $\nu' = \nu_n + \nu_{in} + \nu_{en}\,(m_e/m_i)$

2-10) $U_\alpha = \left[\frac{\gamma\ k\ T_\alpha}{m_\alpha}\right]^{1/2}$ adiabatic speed of sound in α^{th} fluid

where γ = ratio of specific heats, m_α = mass of the α^{th} particle, ε_o = electrical permittivity of free space, and k = Boltzmann's constant.

The following assumptions are also implicit in equation (2-5):

an unbounded medium, no externally generated magnetic field perpendicular to the direction of wave propagation, a fixed percentage of ionization, fluids obeying the ideal gas law and an adiabatic energy equation, and variables of the form usually assumed for a linear theory,

$$2\text{-}11) \quad L'_\alpha = L_\alpha + \ell_\alpha e^{i(kx - \omega t)}; \; |\ell_\alpha| << |L_\alpha| \; .$$

When the neutral density is much greater than the ion density so that

$$2\text{-}12) \quad N_n T_n >> N_e T_e \; ,$$

as it is for all of the experiments to be discussed in this paper, equation (2-5) is valid for all frequencies where

$$2\text{-}13) \quad \omega^2 > \nu_n(\nu_{in} + \nu_{en} (\frac{m_e}{m_i}))$$

except those frequencies which are very close to the plasma frequencies. These special frequencies will not be of interest to us since our experiment is performed at frequencies where $\omega << \omega_i$.

If

2-14) $\nu' << \omega << \omega_i$

we can simplify equation (2-5) to

2-15) $$\frac{k\, U_p}{\omega} = 1 + i\, \frac{1}{2\omega} \left[\nu_{in} + \nu_{en} \left(\frac{m_e}{m_i}\right)\right]$$

where $U_p = \left(\frac{\gamma\, k\, T_e}{m_i}\right)^{1/2}$ is the plasma sound speed with $T_e >> T_i$.

The imaginary part of k, which is independent of ω, is small according to equation (2-15); therefore this dispersion relation represents a wave traveling with slight attenuation per wavelength and with the phase velocity

2-16) $$V_{pH} = \frac{\omega}{Re\, k} = U_p$$

This is the ion-acoustic wave which has been observed by several researchers.[16,17] The ions and electrons participate in this wave with very little coupling to the neutral atoms through collisions.

An ordinary neutral sound wave can also propagate with small attenuation in this frequency range. The dispersion relation for such a wave is

$$2\text{-}17) \quad k^2U_n^2 = \omega^2 + i\omega\nu_n \ .$$

(A third wave solution, $k^2U_i^2 = \omega^2 - \omega_i^2 + i\omega\nu_i$, is also valid in this range, but is not of interest to us because it is damped in extremely short distances).

As the frequency decreases and approaches ν', the phase velocity and the attenuation factor of the ion-acoustic wave described by equation (2-5) decrease. When the frequency is so low that

$$2\text{-}18) \quad \omega^2 << \nu_n(\nu_{in} + \nu_{en}\left(\frac{m_e}{m_i}\right))$$

the correct dispersion equation for this wave becomes

$$2\text{-}19) \quad k^2U_p^2 = i\omega(\nu_{in} + \nu_{en}\left(\frac{m_e}{m_i}\right))$$

or

$$2\text{-}20) \quad k\,U_p \triangleq \left(\frac{\omega}{2}\right)^{1/2} (1+i)\left(\nu_{in} + \nu_{en}\left(\frac{m_e}{m_i}\right)\right)^{1/2}$$

which is identical to the dispersion relation derived by Hatta and Satto in Reference (18).

Equation (2-20) shows that for this wave the damping length is inversely proportional to the square root of the frequency and the phase velocity is directly proportional to the square root of the frequency. This is the only linear plasma wave solution for which the phase velocity can be less than the adiabatic sound speed for the neutral fluid.

In this same limit the neutral sound wave becomes a wave traveling with the sound speed for the total fluid,

$$2\text{-}21) \quad U_T^2 = \frac{\gamma_i P_i + \gamma_e P_e + \gamma_n P_n}{\rho_i + \rho_n + \rho_e} \triangleq \frac{\gamma(P_e + P_n)}{\rho_i + \rho_n} . \qquad (T_e >> T_i)$$

The dispersion relation for this wave is given by

$$2\text{-}22)\quad k^2U_T^2 = \omega^2\left[1 + i\,\frac{\omega(U_T^2 - U_n^2)^2}{\rho\,\frac{\nu_n}{\rho_n}\,U_T^4}\right].$$

When the ion temperature is nearly the same as the neutral temperature, and $N_n\,T_n >> N_e\,T_e$, U_T^2 is of the same order of magnitude as U_n^2 and the damping of this wave is very small. The dispersion relation of equation (2-22) then becomes

$$2\text{-}23)\quad k\,U_T \triangleq \omega\left[1 + i\,\frac{\omega(U_T^2 - U_n^2)^2}{2\rho\,\frac{\nu_n}{\rho_n}\,U_T^4}\right]$$

which shows that the phase velocity is U_T and is independent of frequency, but that the damping length is proportional to ω^{-2}.

2.3 Effect of Drift Velocities

The preceeding dispersion relations were derived under the assumption that none of the fluids had a drift velocity in addition to the velocity due to the wave motion. In the event that the ion and electron fluids are drifting, with drift velocities V_{oi} and V_{oe} (which are both assumed to be much smaller

than U_p), the dispersion relation given by equation (2-15) becomes[24]

$$2\text{-}24)\quad \frac{kU_p}{\omega} = \frac{-\left[\left(V_{oi} + V_{oe}\left(\frac{m_e}{m_i}\right)\right) + i\left(\frac{V_{oi}\,\nu_{in}}{\omega} + V_{oe}\,\frac{\nu_{en}}{\omega}\left(\frac{m_e}{m_i}\right)\right)\right]}{U_p}$$

$$\pm\left[1 + i\left(\frac{\nu_{in}}{\omega} + \frac{\nu_{en}}{\omega}\left(\frac{m_e}{m_i}\right)\right)\right]^{1/2}.$$

The positive sign in equation (2-24) is to be used for the wave propagating in the positive x direction. Writing the dispersion relation explicitly for the waves traveling in the two directions we have

$$2\text{-}25)\quad k_+ = \frac{\omega}{U_p}\left[1 - \frac{V_{oi} + V_{oe}\left(\frac{m_e}{m_i}\right)}{U_p}\right] + i\,\frac{\nu_{in}}{U_p}\left(\frac{1}{2} - \frac{V_{oi}}{U_p}\right)$$

$$+ i\,\frac{\nu_{en}}{U_p}\left(\frac{m_e}{m_i}\right)\left(\frac{1}{2} - \frac{V_{oe}}{U_p}\right)\quad (\text{ positive x direction })$$

and

$$2\text{-}26)\quad -k_- = \frac{\omega}{U_p}\left[1 + \frac{V_{oi} + V_{oe}\left(\frac{m_e}{m_i}\right)}{U_p}\right] + i\,\frac{\nu_{en}}{U_p}\left(\frac{m_e}{m_i}\right)\left(\frac{1}{2} + \frac{V_{oe}}{U_p}\right)$$

$$+ i\,\frac{\nu_{in}}{U_p}\left(\frac{1}{2} + \frac{V_{oi}}{U_p}\right) \qquad \text{(negative x direction).}$$

If $V_{oe} = V_{oi} = 0$, these two equations reduce to equation (2-15). In the experiments to be discussed later, V_{oi} is in the positive x direction and V_{oe} is oppositely directed, while $|V_{oi}| >> |(\frac{m_e}{m_i})V_{oe}|$.

If for this case we write the phase velocities and damping factors explicitly we find

$$2\text{-}27a)\quad \frac{\omega}{R_e k_+} = \frac{U_p}{\left[1 - \frac{V_{oi}}{U_p}\right]} \triangleq U_p + V_{oi}$$

$$2\text{-}27b)\quad \frac{\omega}{R_e k_-} = \frac{U_p}{\left[1 + \frac{V_{oi}}{U_p}\right]} \triangleq U_p - V_{oi}$$

$$2\text{-}28a)\quad \operatorname{Im} k_+ = \frac{\nu_{in}}{U_p}\left(\frac{1}{2} + \frac{V_{oi}}{U_p}\right) + \frac{\nu_{en}}{U_p}\left(\frac{m_e}{m_i}\right)\left(\frac{1}{2} + \frac{|V_{oe}|}{U_p}\right)$$

$$2\text{-}28b)\quad \operatorname{Im} k_- = \frac{\nu_{in}}{U_p}\left(\frac{1}{2} + \frac{V_{oi}}{U_p}\right) + \frac{\nu_{en}}{U_p}\left(\frac{m_e}{m_i}\right)\left(\frac{1}{2} - \frac{|V_{oe}|}{U_p}\right)$$

Thus in this approximation the phase velocity of this wave is equal to the phase velocity of the same wave in a stationary fluid plus or minus the ion drift velocity, depending on whether the wave is traveling with or against the drift motion of the ions.

The damping factors are also modified by the fluid drift velocities, with the higher phase velocity wave having considerably less attenuation than the low phase velocity wave. The phase velocity and damping factor of both waves is independent of frequency, as was the case for $V_{oe} = V_{oi} = 0$.

Only plane wave solutions have been considered in this section. The frequencies at which we perform our experiments are below the cutoff frequency for the mode of propagation which is found by including the effects of the finite discharge tube radius. Thus we have assumed that only plane waves will propagate, a situation which is analogous to having ordinary

plane sound waves in a tube whose diameter is small compared to the wavelength.[16,17,27]

2.4 Finite Pressure Waves and Shock Waves

In this section we consider one-dimensional pressure waves of finite amplitude and shock waves in terms of a single-fluid model as presented by Landau and Lifshitz in Reference (15).

The sound speed for an infinitesimal amplitude sound wave, $C_o^2 = \frac{\gamma P_o}{\rho_o}$, is a first order solution to the equation for sound wave propagation. Higher order solutions are not important because the small amplitude wave is attenuated by viscous damping or thermal energy loss before the higher order terms can have any effect on its motion.

When the amplitude is large enough it becomes necessary to include higher order terms in the solution of the wave equation. The situation can be described physically by considering a pressure pulse of finite amplitude and width. Because the pressure is greatest at the peak of the pulse, the speed of sound in the fluid at the position of the peak is greater than the sound speed for elements of fluid to either side of the peak. As a result, the pulse tends to become more sharply peaked spatially, a process which continues until

a shock wave is formed. If the initial sound wave is sinusoidal with a wavelength λ_o and frequency ω_o, the shock fronts which develop will be a distance λ_o apart. Until the time that the shock has formed, any point on the profile of the wave will travel with a velocity $u = c_o \pm v$ where v is the velocity of the fluid through which the wave is propagating.

A Fourier analysis of the steepening wave will show that as it becomes steeper, higher Fourier components appear at frequencies which are multiples of the fundamental frequency ω_o.

If the initial amplitude is such that a "weak" shock develops, the shock velocity in a perfect gas will be given by $u = c_o + \frac{1}{2}(\gamma + 1)\, v$.

The shock front which develops through the above process is in fact defined by a surface of discontinuity through which the fluid pressure, velocity, and density are discontinuous functions of position. The thickness of this shock front is determined by the strength of the shock.

Another type of discontinuity surface is known as a "weak" discontinuity. It is characterized by the fact that ρ, v, and P are continuous but one or more of their spatial derivatives are

discontinuous or infinite across the surface. Unlike the shock wave, a weak discontinuity travels with the local speed of sound, each point on the wave profile propagating in the same manner as in a linear wave, which results in a spreading of the discontinuity as time advances. These weak discontinuities cannot develop without a stimulus external to the wave such as a singularity in the time variation of the fluid flow.

A single fluid model has been considered in this section because our experimental results indicate that the ions and electrons are strongly coupled to the neutral atoms. In this case v, the drift velocity of the fluid to which we have referred in the previous discussion, is given by

$$2\text{-}29) \quad v = \frac{\rho_i v_{oi} + \rho_e v_{oe} + \rho_n v_{on}}{\rho_i + \rho_e + \rho_n} \quad .$$

Since for our experiment $v_{on} = 0$ and $\rho_n >> \rho_{e,i}$ we have approximately

$$2\text{-}30) \quad v \triangleq \frac{n_i}{n_n} \left(v_{oi} + v_{oe} \left(\frac{m_e}{m_i}\right)\right) \triangleq \frac{n_i v_{oi}}{n_n} << 1 \quad .$$

This relation shows that if we include a drift velocity in our analysis, it can only result in a slightly increased velocity for a finite wave or weak shock wave which travels in the direction of the ion drift.

CHAPTER III

EXPERIMENTAL EQUIPMENT AND DISCHARGE TUBE OPERATION

3.1 Introduction

The experimental equipment, Figures (3-1) and (3-2), consists of two systems; one system including those components necessary to maintain the discharge, and the other composed of apparatus used for monitoring and recording data. The major components of these systems are described in this chapter.

3.2 Discharge Tube

The discharge tube is constructed of three sections which are joined together by O-ring seals. It has a 5 cm. I.D. and an anode-to-cathode length of 66 cm. Complete dimensions are given in Figure (3-3).

The cathode section contains the cathode, a fixed tungsten grid, and a port used to evacuate the tube and to admit argon gas. An oxide coated cathode from a 6011 thyratron is used. These cathodes, which can emit several amperes, are supplied by the General Electric Company. The center section is a piece of Pyrex tubing with O-ring flanges at both ends. By using center sections of different lengths, the overall length

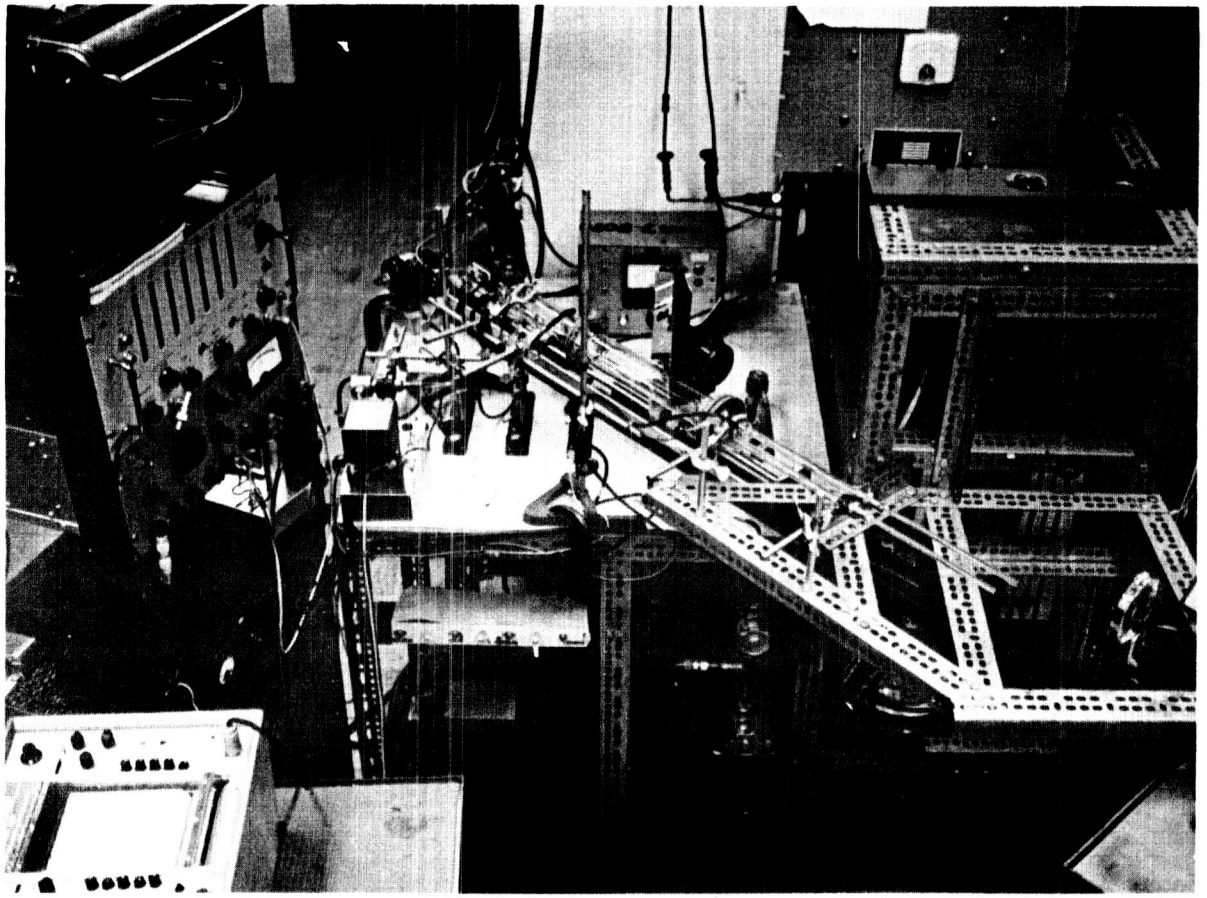

Fig. 3-1. Photograph of Equipment

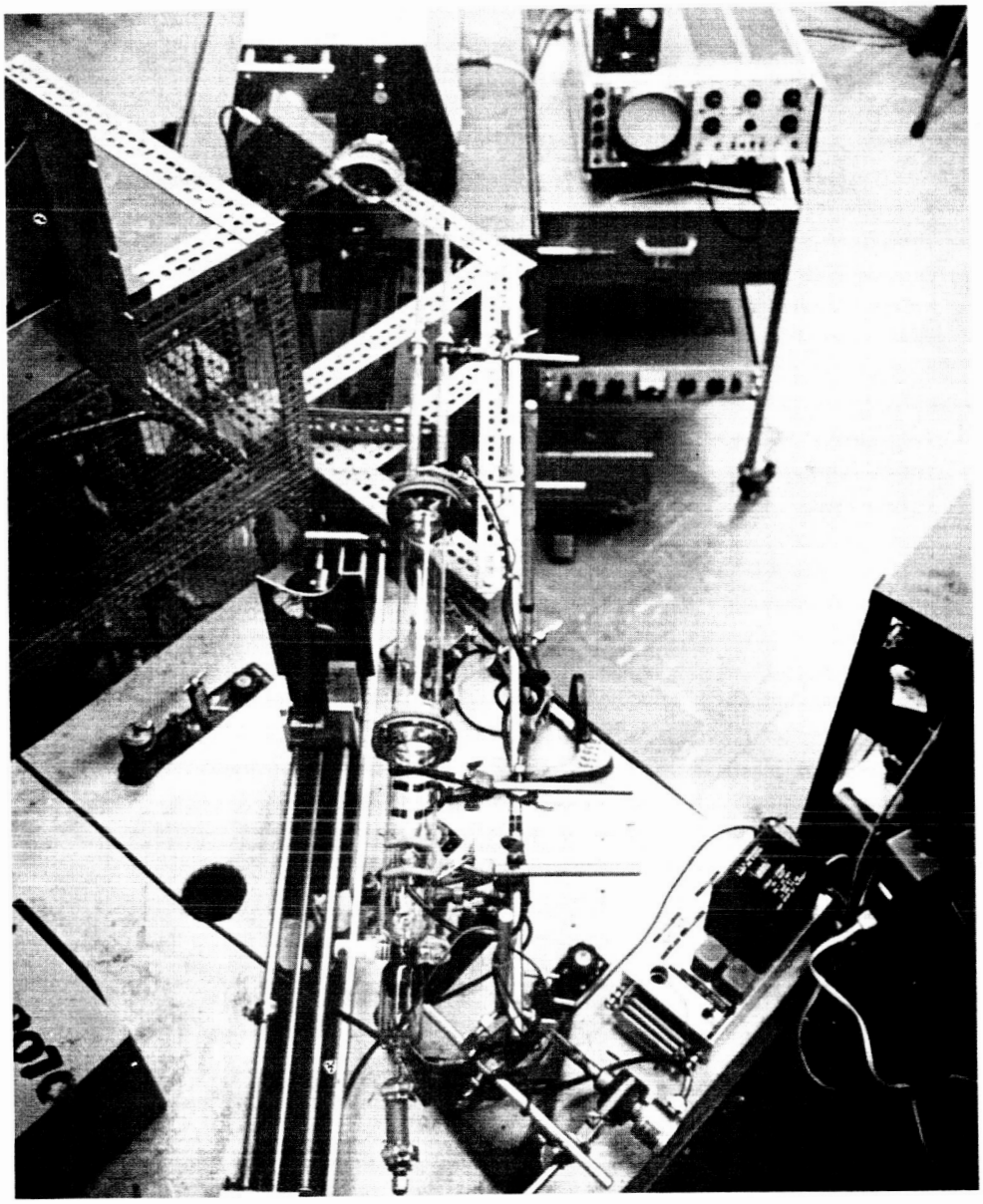

Fig. 3-2. Photograph of Equipment

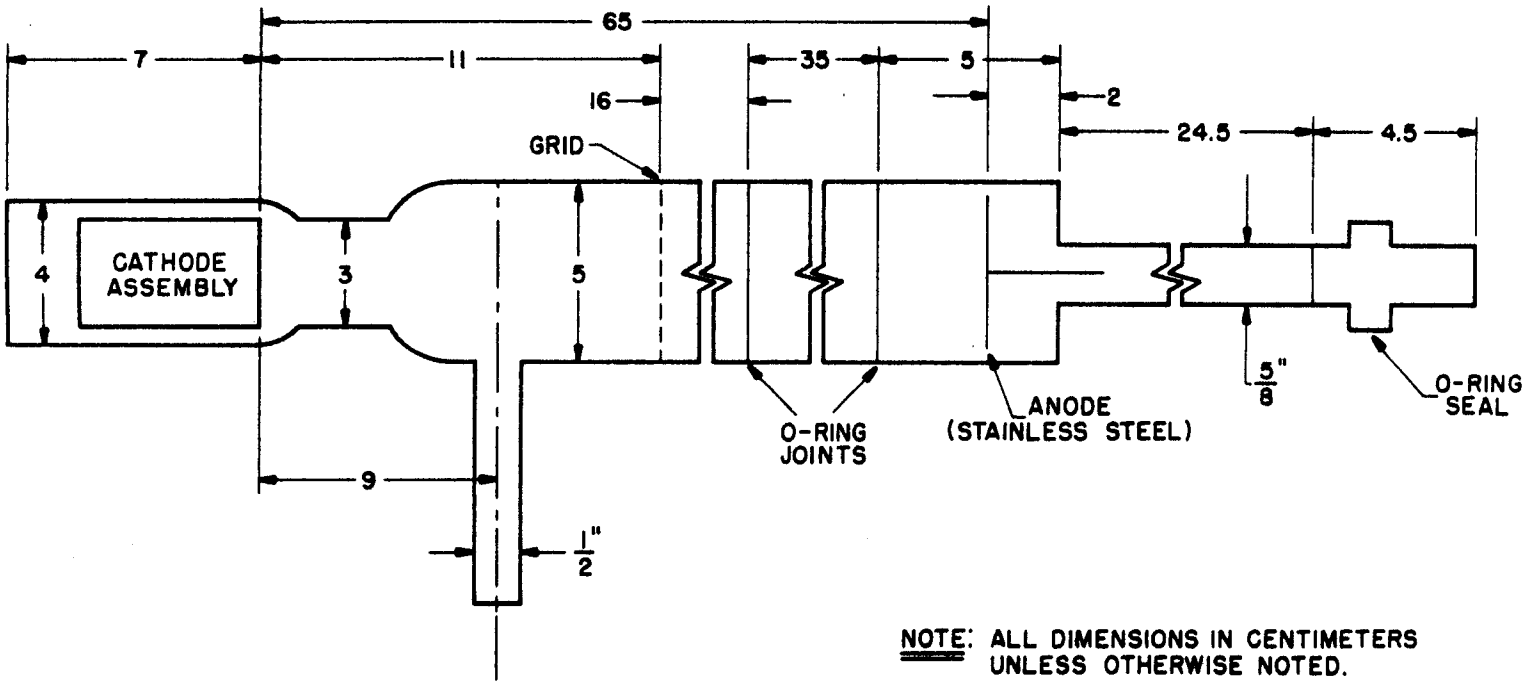

FIG. 3-3 SCHEMATIC OF DISCHARGE TUBE.

of the discharge tube can be easily changed.

The anode section has two 5/8 in. O.D. Pyrex arms extending behind the anode which were necessitated by the type of axially mobile grid and probe employed in the tube. The seals at the ends of the arms, as well as the grid and probe are described in the next section. Support for the discharge tube is supplied by ring stands and clamps.

3.3 Probe, Grids, and Seals

The Langmuir probe was made by fusing .01 in. diameter tungsten wire into .125 in. pyrex tubing via a uranium glass seal.

The movable and stationary grids are of identical construction. A tungsten rectangular grid of .001 in. wires with .030 in. between adjacent wires was spot welded to a nickel ring which provides circumferencial support and a means for fastening the grids to the electrodes which hold them in position.

An electrode for the fixed grid is inserted through the wall of the discharge tube 11 cm. from the cathode, while the electrode for the movable grid is fused into a piece of pyrex tubing like that used for the probe.

The two pieces of .125 in. tubing which support the probe and movable grid extend from the discharge region past the anode and into the extension arms of the anode section. There the tubing is fused to the .375 in. O.D. precision ground tubing which is the reciprocating member of the O-ring seal at the end of each arm.

These two-piece O-ring seals each have two internal O-ring grooves, a geometry which requires the inside diameter of the seal to be large enough so that O-rings can be inserted without excessive difficulty; hence the choice of .375 in. tubing. Since the .375 in. tubing cannot extend past the anode, the total axial movement available to the probe and grid is the same as the distance between the anode and the seals; 28 cm.

3.4 Vacuum System and Gas Supply

The vacuum system consists of a 2 in. air cooled oil diffusion pump with a water cooled baffle, and a 5 cu. ft/min. mechanical roughing pump. This arrangement provides a static base pressure of less than 4×10^{-6} torr. in the discharge tube, as measured by a cold cathode ionization gauge. When the probe or grid are moved through their maximum displacement with constant but moderate speed the pressure of the system remains below 10^{-5} torr. and returns to the base pressure

within 30 seconds. During a data run the probe is moved in 2 cm. increments and the recovery time is at most a few seconds.

The usual operating pressures of the discharge, 10^{-2} to .5 torr. are in a range of poor accuracy for the cold cathode ionization gauge, so a Pirani gauge is used to measure pressures in this range. Two calibration compensations are necessary; the first because the Pirani gauge is calibrated for air, and the second because the discharge is normally run with a continuous flow of argon through the tube. The first correction is made by obtaining the true pressure for argon from a graph supplied by the gauge manufacturer. The second correction is accomplished by running the discharge with and without a flow of argon. For a given indicated pressure in the flowing system, the discharge tube voltage and current and the frequency of the striations are recorded. (The striation frequency is particularly sensitive to the pressure.) Measuring the pressure while running the tube at the same voltage, current, and striation frequency with no gas flow then gives the corrected pressure reading.

The flowing system is used to insure that the purity of the gas is maintained over long time intervals. O-ring seals cannot be made absolutely tight, and if the flowing system were not used the ratio of argon to other gases within the tube

would decrease significantly within times on the order of hours. To control the flow of argon an Edwards leak valve is used between the argon cylinder and the discharge tube.

3.5 Power Supplies

The anode voltage is provided by a regulated D.C. supply rated for .5 amperes at 0-600 volts. A series connection of three 250 ohm resistors, together with a total of 60 mf. capacitance, provides a total load resistance of 750 ohms plus RC filtering in addition to that of the power supply. The cathode heating current, usually 11 amperes, is provided by a battery-eliminator type D.C. supply with an output of 15 amperes, and 0-12 volts.

A third power supply which is sometimes used to provide D.C. bias on the grids is rated at .15 amp, 0-500 volts.

3.6 Phase Sensitive Detection System

A lock-in amplifier (LIA) provides a complete phase sensitive detection system including frequency selective tuning and amplification in a signal and a reference channel, a mixer-modulator, a low-pass filter and detector, and output circuits suitable for driving data-recording devices. The

LIA allows one to detect a weak signal in the presence of strong background noise by amplifying the frequency components of the input signal which are frequency and phase coherent with respect to the reference channel signal. Various modes of operation are possible, but only the mode normally used for this experiment will be described.

A reference signal of the same frequency as the modulation of the discharge tube plasma is applied to the reference channel. This reference signal can be obtained from the current in the external circuit when spontaneously generated disturbances are being studied, from an external oscillator if the voltage of one of the grids is being modulated, or, for any type of modulation, from another grid or probe in the plasma. The LIA is tuned to this frequency and the reference signal is amplified to drive the mixer-modulator.

Input signals can be taken from the output of a photomultiplier tube, a probe, or a transformer used to measure a-c currents in various portions of the external circuit. The frequencies of the signal which correspond to the reference frequency are filtered and amplified in the signal channel of the LIA before entering the mixer-modulator, whose output is at the sum and difference of the signal and reference frequencies. Since the difference frequency is zero, (d-c), a

low-pass filter is used to separate the sum and difference frequencies. The amplitude of the d-c component is converted to a voltage which can be read on a panel meter or used to drive a chart recorder. This output voltage is proportional to the amplitude of the input signal at the reference frequency and to the cosine of the phase angle between the signal and reference waveforms; hence the term "phase sensitive detection". An adjustable phase shifter in the reference channel allows one to maximize or minimize the cosine of the phase angle.

3.7 Optical System

The input signal to the LIA usually comes from the output of a photomultiplier tube (P.M.) which is used to monitor the light intensity of a particular region of the discharge. Dumont 6467 photomultiplier tubes are used with a 10K load resistor and 1.3 KV across the tube. The photomultiplier can be mounted on a grating monochromator when it is desirable to look at the light output at a particular wavelength or can be mounted so as to monitor the total light output. In either case, the light is focused on the plane of the monochromator entrance slit by means of the lens and mirror system shown in Figure (3-5). A mirror and 8 in. focal length lens are mounted

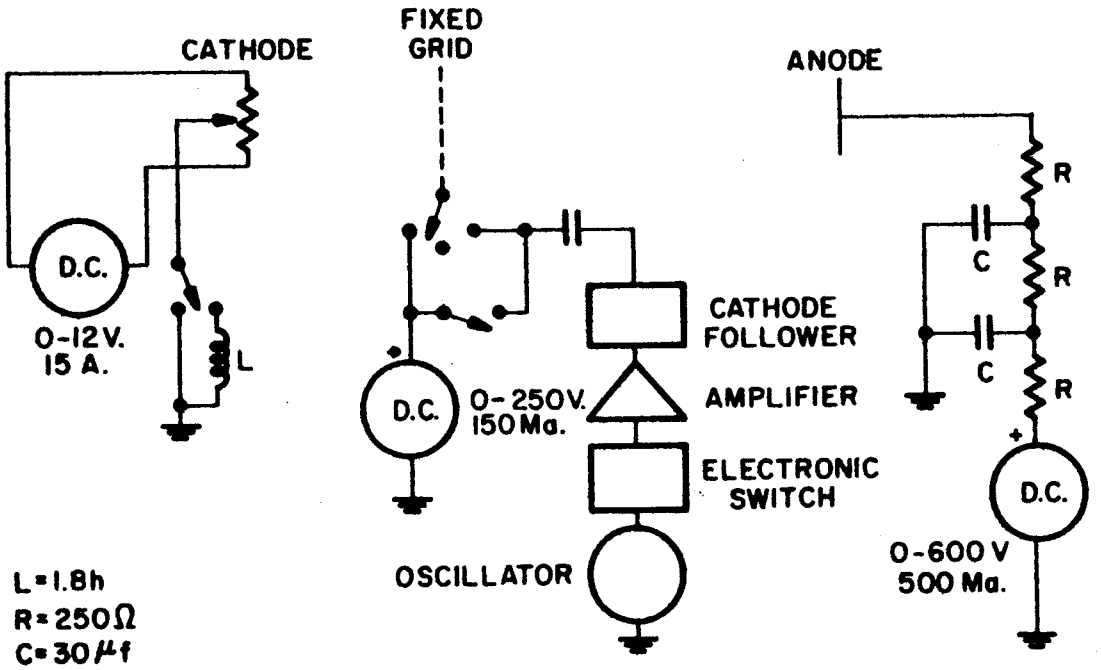

FIG. 3-4 DISCHARGE TUBE ELECTRICAL CIRCUIT.

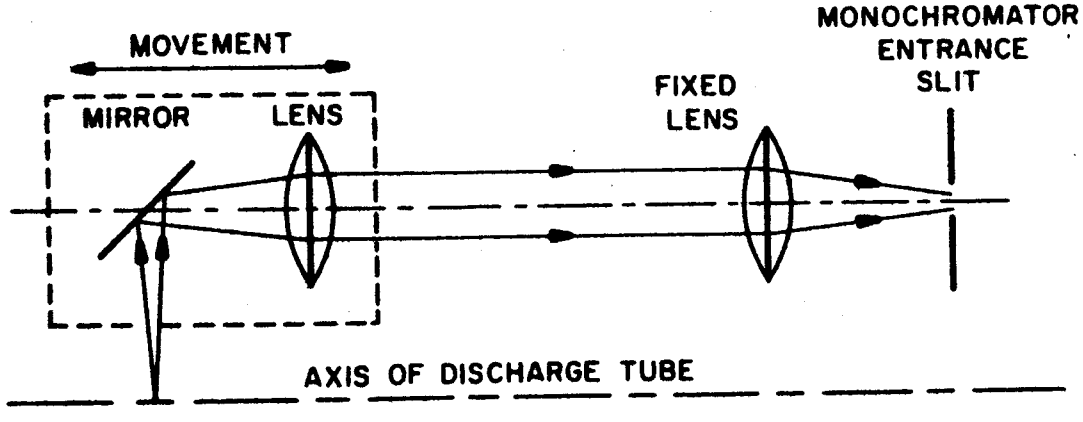

FIG. 3-5 SCHEMATIC OF OPTICAL SYSTEM.

on a carriage which is moved parallel to the axis of the discharge tube by an electric motor. The focal point of the lens is on the axis of the discharge tube. Parallel light emerging from the movable lens is gathered by a stationary lens and focused on the plane of the entrance slit. This arrangement keeps the light focused on the slit as the mirror and lens traverse the length of the tube. The region of the discharge contributing to the light is approximately a thin plane perpendicular to the discharge tube's axis. For an entrance slit width of 50 microns, the width of this plane is less than 1 mm. Care is taken in alignment of the mirror to insure that the plane observed is not skewed with respect to the tube axis.

3.8 Qualitative Description of Discharge Tube Operation

3.8.1 D.C. Effects

The quantitative understanding of the consequences of inserting a grid which is biased to some D.C. potential into a gas discharge is in itself a problem of considerable complexity and is outside the scope of this paper. The philosophy which was adopted with regard to the grids was that they are to be considered as auxiliary devices which can possibly help to create conditions within the positive column which are favorable

to the study of plasma waves. Therefore, we did not attempt a quantitative survey of the effects of the many possible combinations of grid bias and position; however, certain qualitative effects were sought. It was hoped that proper biasing of the grids could increase the axial uniformity of the plasma between the two grids and reduce the noise amplitude. It was also hoped that the grids would provide clearly defined boundaries for plasma wave propagation in the tube. These hopes were fulfilled to a limited extent as will now be described, considering first the general D.C. behavior of the discharge with the grids present. This description refers specifically to a discharge running with 76 volts from cathode to anode, 500 ma. discharge current, and a pressure of 8×10^{-2} torr., but is typical of the operation within the investigated range of pressure and currents.

Surrounding the cathode is the cathode glow, a region of moderate light intensity which gradually diminishes with distance from the cathode. Another region of moderate intensity, the negative glow, begins approximately 6 to 7 cm. from the cathode and diminishes into the Faraday dark space which extends to the fixed grid 11 cm. from the cathode (the dimensions in this section refer to the tube as shown in Fig. (3-3)). Adjacent to the anode side of the grid is a region of high light

intensity. This region extends for about 2 cm. where it seems to become a second Faraday dark space. The luminous negative end of the positive colmun begins about 6 cm. from the fixed grid. The first several centimeters at this end of the positive column are not uniformly intense, but at 8 to 10 cm. from the end, the uniform column begins and extends to the movable grid. The region on the anode side of the movable grid is similar to the corresponding region at the fixed grid—a few centimeters of high light intensity followed by a "Faraday dark space", and then another portion of the positive column which extends to the anode.

A decrease in pressure results in a decrease in the length of the positive column, while a decrease in current causes a slight shortening of the positive column and a reduction of the light intensity in all regions of the discharge.

The intense regions on the anode side of both grids is probably due to an acceleration of the electrons as they flow through the grids on their way to the anode. Within a few centimeters they lose their added energy by colliding with neutral gas atoms and are then accelerated again in the dark space until they gain enough energy to excite neutral argon atoms. The region where this energy is attained is the start of the positive column.

When either grid is biased negatively with respect to the plasma, the discharge tries to bypass the grid by going through the space between the grid and the wall of the tube.

Positive biasing of the grids results in electron current being drawn from the discharge. Since the cathode is capable of providing at least twice the maximum anode current (500 ma.), the anode current remains almost constant even when several hundred milliamperes are being collected by the grids. Current drawn by the fixed grid does not have an appreciable effect on the d-c behavior of the positive column. Increasing the current collected by the movable grid causes increased luminosity of the positive column on the cathode side of the grid.

Since we observed no significant advantage of operation with the grids connected to the external circuit, most of the measurements reported in Chapter 4 were made with both grids floating and the movable grid positioned 7 cm. from the anode.

3.8.2 A.C. Effects

When the positive column which visually appears to be steady and uniform is observed by means of the photomultiplier tube as described in Section 3.7 it is found that the light intensity at any point in the column shows rapid variations in

time. The regularity of the variation with time depends on whether an inductance is placed in the cathode circuit as shown in Figure (3-4). Figure (3-6) illustrates the photomultiplier output voltage with and without the inductance in the circuit. Our experiments show that the fundamental frequency of the striations is not determined by the inductance or other external circuit parameters, a result which agrees with those of other investigators. When the inductor is absent the frequency spectrum is spread more broadly about the fundamental and harmonic frequencies.

The striations are observed to spread spatially as they travel away from the anode (Figure 3-7). This spreading, which is also seen in the Fourier analysis of Section 4-2, does not seem to have been observed in other striation experiments.

The voltage across the cathode circuit inductance shows peak-to-peak variations on the order of 10 volts. Despite this large voltage variation (L di/dt), it is known that the amount of current participating in each Fourier frequency component is on the order of tens of microamperes, an amount which is very small compared to the total discharge current, which is at least 350 milliamperes (Figure 3-8).

As the presence of the inductance did not change the

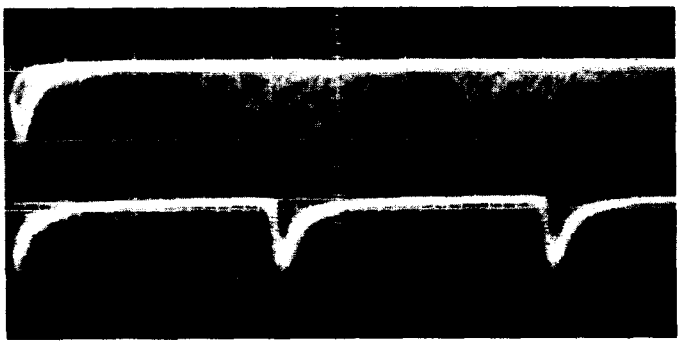

Upper Trace: Photomultiplier Output,
Cathode Grounded
Vertical: 50 mv/div
Horizontal: 100 μs/div

Lower Trace: Photomultiplier Output,
Inductor in Cathode Circuit
Vertical: 50 mv/div
Horizontal: 100 μs/div

Pressure: .08 Torr.
Discharge Current: 500 ma.

Fig. 3-6. Effect of Inductor in Cathode Circuit

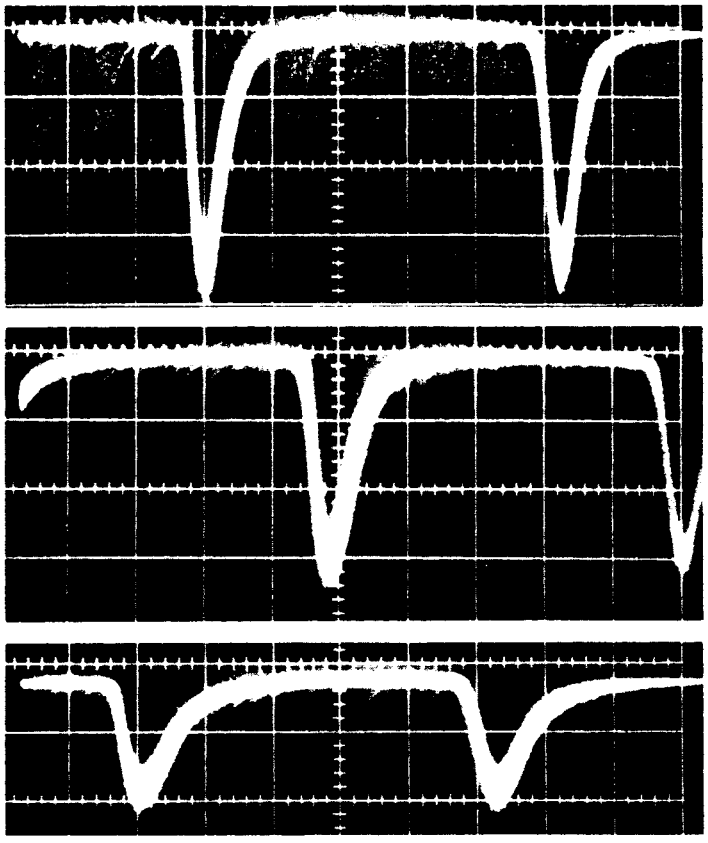

Photomultiplier Output
Upper Trace: 10 cm. from anode
Middle Trace: 20 cm. from anode
Lower Trace: 30 cm. from anode

Horizontal (All Traces): 50 μs/div
Vertical (All Traces): 20 mv/div

All traces were triggered from constant external signal (Cathode inductor voltage). Pulses occur later in time as point of observation moves away from anode.

Fig. 3-7. Variation of Light Pulses with Distance from Anode

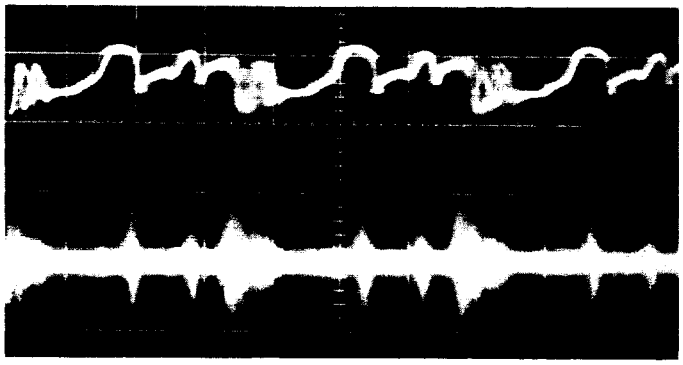

Upper Trace: Voltage Across Cathode Inductor
Vertical: 20 v/div
Horizontal: 100 μs/div

Lower Trace: A.C. Current in Anode Circuit
Vertical: 10 ma/div
Horizontal: 100 μs/div

Pressure: .08 Torr.
Discharge Current: 500 ma.

Fig. 3-8. Cathode Voltage and A.C. Anode Current

frequency of the striations, nor, we assume, the propagation of the striations through the positive column, it was advantageous to make our measurements with the inductance in the circuit. The resulting regularity of the striations greatly simplified the time synchronization of many of our measurements.

CHAPTER IV

MEASUREMENTS AND RESULTS

4.1 Introduction

The measurements described in this chapter were taken while operating the discharge tube with Argon gas at pressures between .02 and .48 torr. For this range of pressures the fundamental frequency of oscillation was approximately proportional to $p^{-3/4}$. An increase of the discharge current at a given pressure causes a decrease in the fundamental frequency. The pulses of external circuit current associated with the striations were a small part of the total discharge current (10 ma. peak compared to 500 ma. total)(Figure 3-7). Both of these observations agree with those of Donahue and Dieke.[1]

Our most complete set of data was taken at a pressure of .08 torr. The very regular behavior of the striations at this pressure was typical of the tube operation for pressures between approximately .04 and .25 torr. Outside of this range the measurements were made more difficult because of an increase in the aperiodicity of the striations.

In order to orient the reader with respect to the order of

magnitude of various plasma parameters we list the following values which are appropriate for our discharge tube operating at a gas pressure of .08 torr.

$p = .08$ torr. $\quad T_e \tilde{=} 1.5$ eV

$T_{i,n} = 300\ ^{\circ}K$ $\quad N_{i,e} \tilde{=} 2 \times 10^{10}$ cm.$^{-3}$

$N_n = 2.6 \times 10^{15}$ cm.$^{-3}$ $\quad m_e/m_i \tilde{=} 1.4 \times 10^{-5}$

$I/A \tilde{=} .27$ ma./cm.^{2} $\quad \nu_{en} \tilde{=} 1.5 \times 10^8$ sec.$^{-1}$

$\omega_e^2 \tilde{=} 6.4 \times 10^{19}$ rad.^{2} sec.^{2} $\quad \nu_{in} \tilde{=} 1.5 \times 10^5$ sec.$^{-1}$

$\omega_i^2 \tilde{=} 8.8 \times 10^{14}$ rad.^{2} sec.^{2} $\quad L_{in}(\text{mfp}) \tilde{=} 3 \times 10^{-2}$ cm.

$L_{en}(\text{mfp}) \tilde{=} 6 \times 10^{-1}$ cm.

4.2 Measurement of the Striation Velocity and Amplitude

Using the frequency selective properties of the LIA enabled us to determine that the same fundamental and harmonic frequencies were present in the photomultiplier and negatively biased Langmuir probe signals as in the ac current in the external circuit. This allowed us to use the voltage across the cathode circuit inductor as the reference signal for the LIA.

The output voltage from the photomultiplier tube or the movable Langmuir probe was connected to the LIA signal channel

and the relative amplitudes of the Fourier components of these signals were determined in the following manner.

The LIA was tuned to the frequency of interest and the LIA phase shifter adjusted until we obtained a maximum reading on the LIA panel meter. This was equivalent to setting the cosine of the phase angle between the signal and reference voltages equal to one; therefore the meter reading gave the amplitude of that Fourier component directly (in arbitrary units).

The time delay introduced into the reference channel by the phase shifter was measured using the circuit of Figure (4-1). An audio oscillator providing a signal at the frequency to which the LIA was tuned was connected to the reference channel of the LIA and to channel B of the EPUT meter.* Channel A of the EPUT meter received the output of the LIA reference channel. The time delay in micro-seconds was obtained directly from the EPUT meter by operating it in the (B-A) mode. It was necessary to check the triggering level of the EPUT meter at each frequency to insure that the indicated time delay agreed with the phase shift measured by means of a Lissajous figure which was displayed on an oscilloscope. The oscilloscope connection is

* EPUT is an acronym for Events Per Unit Time. An EPUT meter is a versatile dual channel triggered counter.

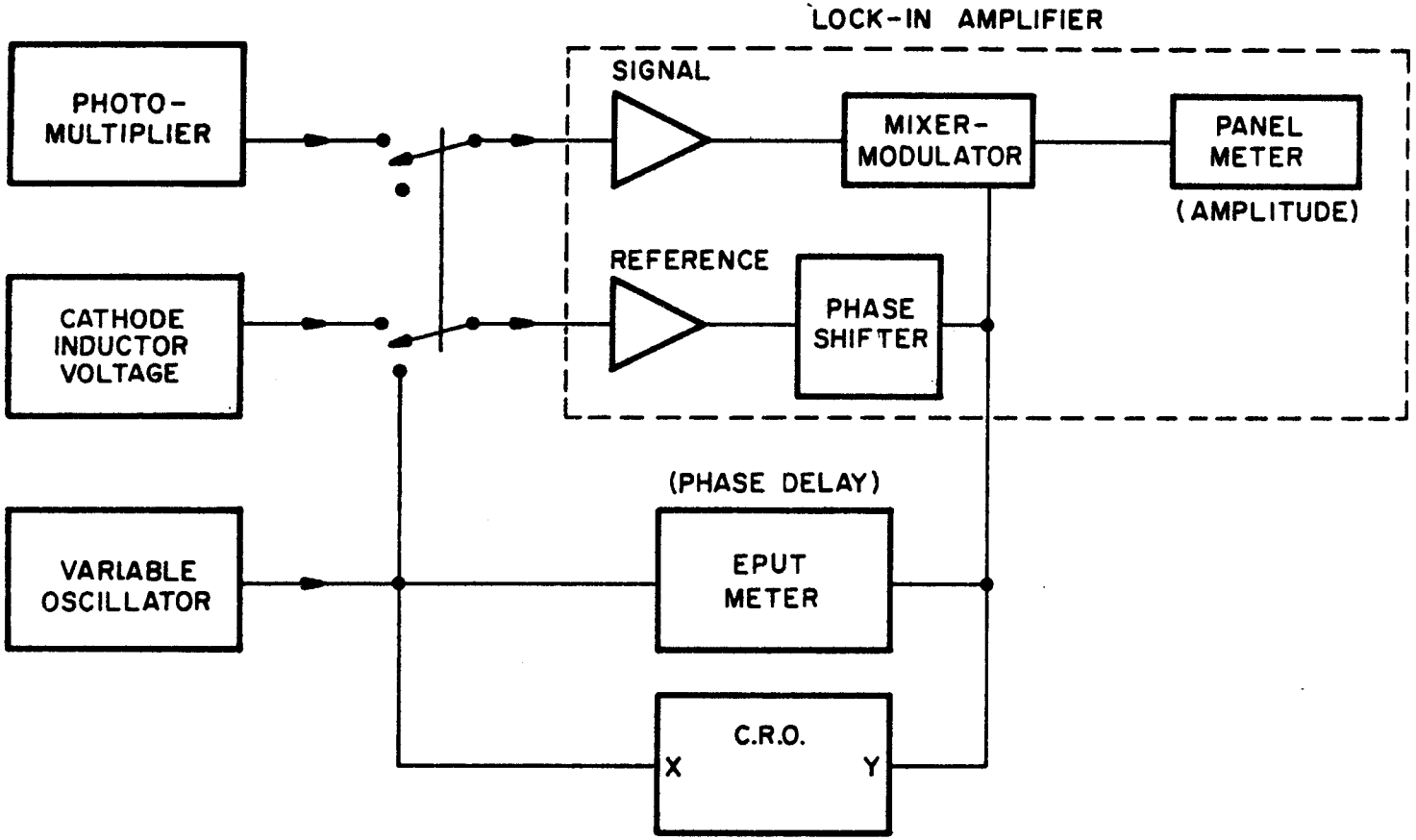

FIG. 4-1 LOCK-IN AMPLIFIER AND ASSOCIATED COMPONENTS.

also indicated in Figure (4-1).

These measurements of amplitude and phase delay were repeated at intervals of two centimeters along the tube axis. The photomultiplier output pulses shown in Figure (3-7) and Figure (4-6) are typical of the pulses which were analyzed. The rise times of these pulses are slower than the response of the photomultiplier output circuit.

The velocities of the striations were found by plotting the phase delay time versus the position along the tube. The reciprocal of the slope of the resulting curve then gives the velocity. Plotting the LIA meter reading versus position for the fundamental and harmonic frequencies gives an indication of the behavior of the amplitude of each Fourier component of the striation as the striation propagates through the positive column.

The data given in this section was taken with the photomultiplier monitoring the neutral argon emission at 4200 angstroms (excitation energy 14.50 e.v.). A number of these same measurements were made with the photomultiplier monitoring the total light emission and with the negatively biased Langmuir probe monitoring changes in the ion saturation current. The velocities and relative amplitudes of the striations as measured

with these two different detectors agreed well with the measurements made using the 4200 Å line. On this basis we concluded that the charged particle and neutral atom motion was closely coupled, and that it was not necessary to make the measurements with each of the three types of detection. Monitoring the 4200 Å line was chosen in preference to using the probe since there could be no question of disturbing the plasma with the detector, and in preference to monitoring the total light output because we felt that it was desirable to define the source of light emission as well as possible.

A set of the phase delay and amplitude curves showing the behavior of the fundamental and 3 harmonic frequencies at a gas pressure of .043 torr. and a discharge current of 500 ma. is shown in Figures (4-2) and (4-3). In Figure (4-2) the curves have arbitrary time (vertical) axis intercepts. These curves are representative of the quality of the data which was obtained at other pressures and currents. Since the slopes of the curves in Figure (4-2) are not constant, it is clear that in this case the striations are slowing as they move away from the anode. At pressures above approximately .1 torr. the slopes were constant over the axial distance observed. Table (4-1) gives the striation frequency and velocity for various pressures and currents. A double entry for the velocity indicates that the slope of the

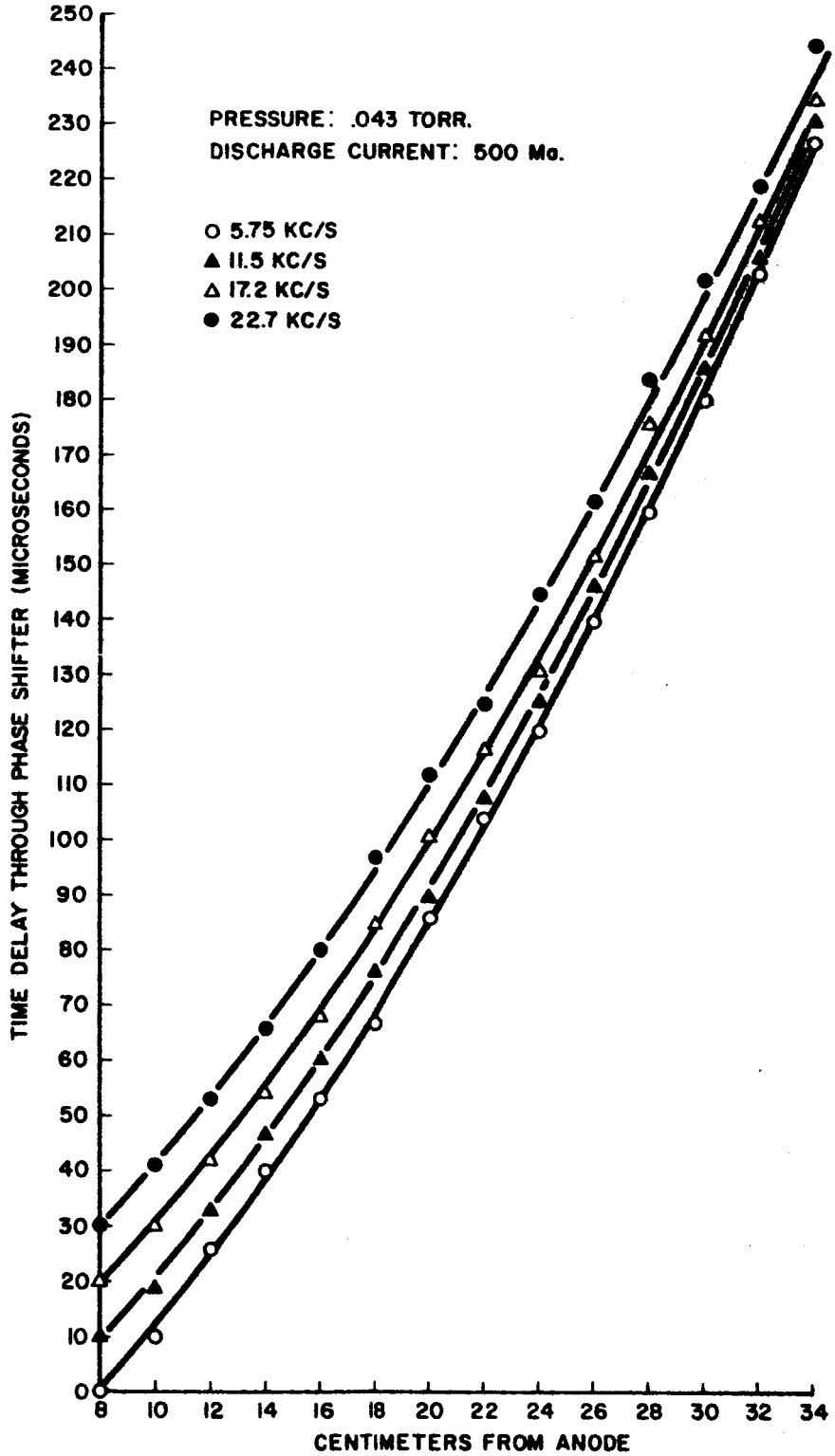

FIG. 4.2 TIME DELAY VERSUS DISTANCE.

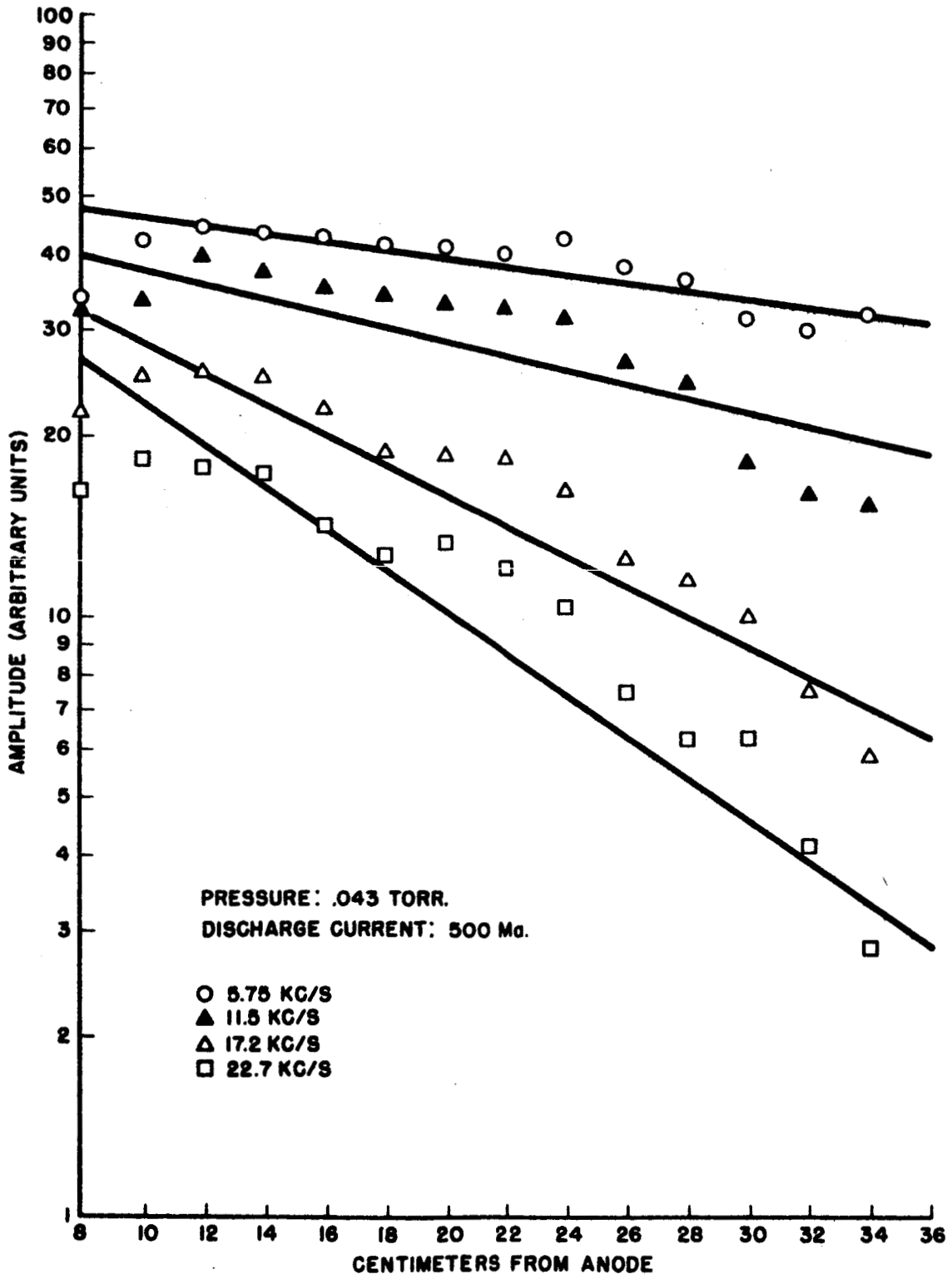

FIG. 4-3 AMPLITUDE (ARBITRARY UNITS) VERSUS DISTANCE.

TABLE 4-1

STRIATION VELOCITY AND FREQUENCY

Pressure (Torr.)	Discharge Current (Ma.)	Frequencies Measured (Kc/s)	Velocity V x 10^{-4} cm/sec.
.043	350	6.9 13.7 20.8	21.0; 11.5
.043	500	5.75 11.5 17.2 22.7	15.1; 9.44
.08	350	3.64 7.25 14.3	10.7; 7.2
.08	500	4.18 8.41 12.7 16.7 20.8	13.0; 8.34
.16	350	1.95 3.9 7.8	3.75
.16	500	2.27 4.54 6.84 9.1 11.4	5.3
.25	350	.667 1.34 2.0	1.29
.25	500	1.42 2.88 4.32	3.04
.48	500	.885	1.81

time delay versus distance curve was not constant. The larger number represents the asymptotic value of the velocity near the movable grid, while the smaller number gives the asymptotic value at the position of observation most distant from the grid.

Our data indicates that the velocity is nearly proportional to p^{-1} instead of $p^{-1/2}$ as found by Coulter.[10] We do not attach much significance to this discrepancy since Coulter quotes an experiment previous to his which also indicated that the velocity is proportional to p^{-1} (Whiddington, Reference (22)). Whiddington's experiment was done in argon, as was ours, while Coulter used neon.

The amplitude versus distance curves in Figure (4-3) show that the amplitude of the various Fourier components do not decay smoothly. They do show the tendency for higher harmonics to damp more rapidly which results in the observed spreading of the pulse. In order to obtain numbers for the attenuation distances which could be compared with theory (in Section 5.2), we drew the solid lines shown super-imposed on the curves. The values which were obtained are only intended to indicate a lower limit for the damping length.

4.3 Measurement of Electron Temperature and Density

The well known theory of the single Langmuir probe allows us to determine the electron temperature and density from the current-voltage characteristics of a collector inserted into the plasma.[20] One determines the electron density by finding the slope of the curve which is obtained by plotting the square of the electron saturation current to the probe versus the probe voltage. For a cylindrical probe the square of the density is given by

$$4\text{-}1) \quad N_e^2 = \frac{\pi^2 m_e}{2e^3 A_p^2} \frac{d(i_{es}^2)}{dV} ; \quad \frac{d(i_{es}^2)}{dV} \triangleq \text{constant}$$

where i_{es} is the electron saturation current and A_p is the surface area of the cylindrical probe.

To determine the electron temperature, one makes a semi-log plot of the electron current versus the probe voltage (not in the saturation region of the probe characteristic). The slope of this curve should be a constant given by

$$4\text{-}2) \quad \frac{d(\ln i_e)}{dV} = - \frac{e}{k T_e} \triangleq \text{constant} .$$

Despite the apparent simplicity of equations (4-1) and (4-2), there are many subtleties involved in obtaining meaningful probe data. The two which were of most concern to us were the necessities of taking the entire probe curve in the absence of plasma oscillations and over a time interval during which the density and temperature remained reasonably constant. Both of these requirements were satisfied by devising the probe circuit shown in Figure (4-4) which allowed us to obtain the entire probe curve in a time interval which was small compared to the period of the striations.

The timing is initiated by obtaining a trigger from the voltage across the cathode inductor and using this trigger to synchronize time base A, which determines the repetition rate at which the curves are taken. Time base A then supplies a delayed trigger to time base B which determines the probe voltage sweep rate. The time delay of the trigger pulse from time base A is continuously variable. This allows one to take the probe curve at any time during the period of the striation. The voltage ramp from time base B goes to the simple cathode follower which then drives the probe circuit shown in Figure (4-4). By driving the horizontal deflection plates of the type 555 oscilloscope with the probe voltage and displaying the probe current on the vertical axis we obtained a direct

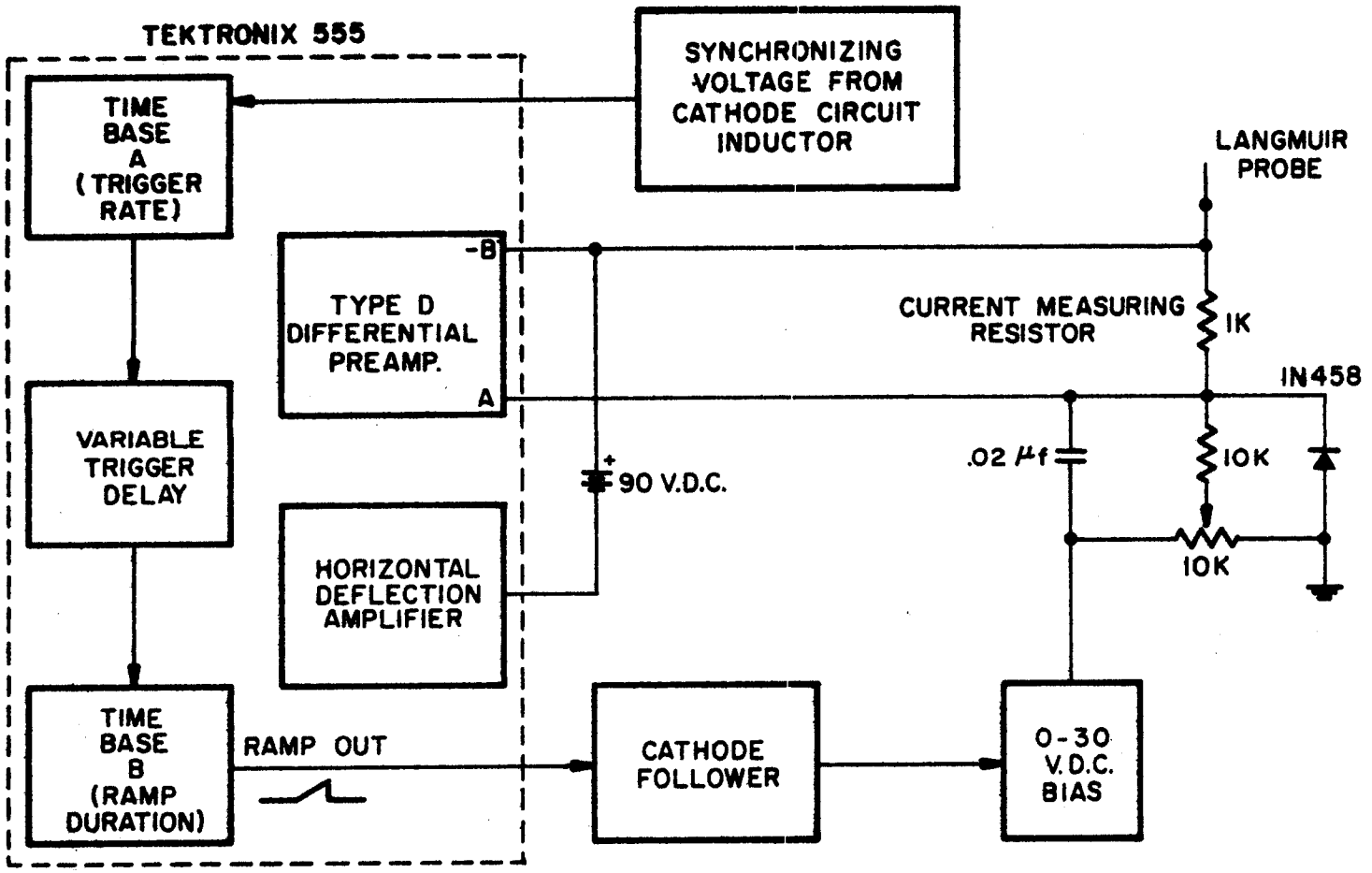

FIG. 4-4 PROBE CIRCUIT---TIMING AND MEASURING.

plot of the current-voltage characteristic. The frequency response of the horizontal deflection amplifier was the limiting factor in obtaining fast probe curves from this system. Even so, the data of this section was obtained from probe curves which were taken in less than 20 microseconds.

Figure (4-5) shows two probe curves together with the photomultiplier output. In each case the photomultiplier was monitoring the plasma at the position of the probe. The intensified region of the photomultiplier trace is the actual total sweep time for the probe voltage, but only for about the last 15 microseconds of this sweep time does the probe collect electron current.

Probe curves were taken immediately after a striation had passed the probe and several microseconds before a striation arrived at the probe. The results of these measurements for various currents and positions in the .08 torr. discharge are given in Table (4-2). Some data is also given for pressures of .043 torr. and .16 torr. to indicate that the electron density and temperature was not strongly dependent on the pressure. For all of the data presented in Table (4-2) the curves which were analyzed according to equations (4-1) and (4-2) displayed quite linear slopes which implies that the electron energies

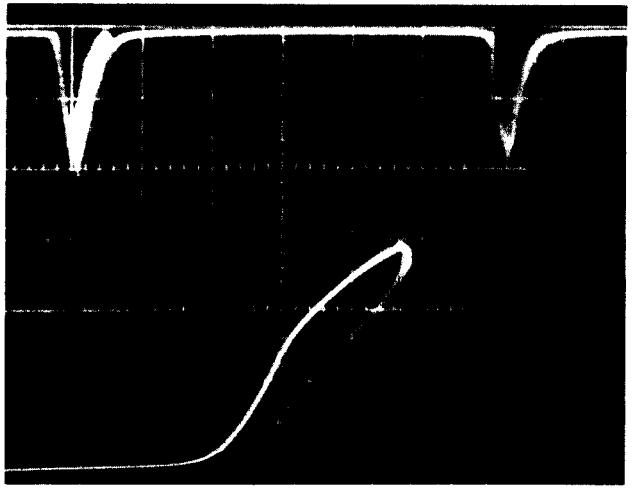

Lower Trace: Probe Curve
Horizontal: 5 v/div
Vertical: 5 ma/div

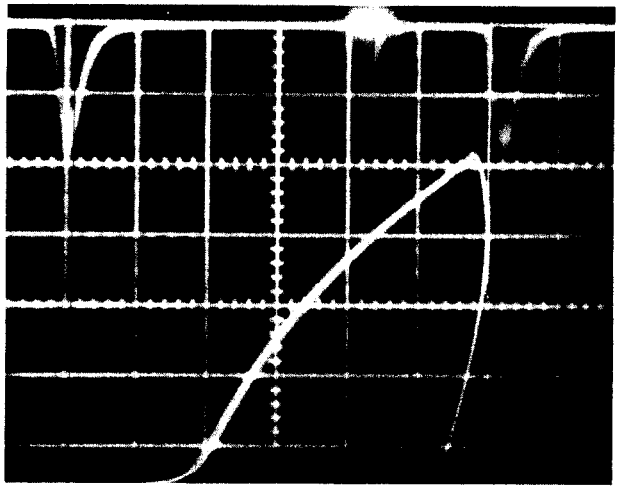

Lower Trace: Probe Curve
Horizontal: 5 v/div
Vertical: 1 ma/div

Data Common to Both Photographs

Upper Traces: Photomultiplier Output; 50 mv/div versus 50 μs/div
Pressure: .08 Torr.
Discharge Current: 350 ma.
Distance from anode: 11 cm.

Fig. 4-5. Langmuir Probe Curves

TABLE 4-2

ELECTRON DENSITY AND TEMPERATURE

Pressure (Torr.)	Distance from Anode (cm.)	Discharge Current (Ma.)	Electron Density and Temperature Immediately Behind Luminous Front		Electron Density and Temperature Before Luminous Front	
			$N_e \times 10^{-10} cm^3$	$T_e \times 10^{-4} °K$	$N_e \times 10^{-10} cm^{-3}$	$T_e \times 10^{-4} °K$
.08	25	500	7.88	2.55	1.47	2.15
.08	25	350	5.72	2.28	1.1	1.21
.08	11	500	7.96	2.02	1.93	1.56
.08	11	350	6.67	2.24	1.5	1.73
.043	25	500	6.82	2.05	1.3	1.92
.16	25	500	7.32	2.24	2.66	1.92

were closely described by the Boltzmann distribution function.[3]

The data of Table (4-2) shows that there is a significant increase in the density and temperature of the electrons associated with the region of enhanced light emission. The density changes by a factor of approximately five as the luminous region passes the probe, a factor which is in very good agreement with the microwave measurements of Sodomsky.[11]

There were certain positions between striations at which reasonable probe curves could not be obtained. The reason for this is not completely understood, but we suspect that it indicates that there are small regions over which the electron density, temperature, and/or plasma potential are changing rapidly. The leading edge of the striation is one of these regions.

4.4 Qualitative Observations of the Effects of Applying an Audio Frequency Signal to the Fixed Grid

When an audio oscillator and cathode follower were used to drive the fixed grid, two effects were observed which were not pursued in detail but which seem interesting enough to warrant their description in this section.

The first of these effects was observed when the inductor was used in the cathode circuit and the naturally occurring striations were thus very regular with a well-defined fundamental frequency. If a variable frequency signal of approximately 20 volts peak-to-peak was applied to the fixed grid, the frequency of the striations became the same as that of the applied signal as long as the applied frequency was not more than approximately twice the natural fundamental frequency.

When the applied frequency exceeded this limit the striations reverted to their natural frequency and only a small amount of the grid signal was seen superimposed on this fundamental frequency.

The second effect was observed with the cathode connected directly to ground. Square wave (on-off) modulation was imposed on the signal from the audio oscillator which was operating at the natural frequency of the striations. The period of the square wave modulation was approximately 6-7 times longer than that of the carrier frequency. A negatively biased Langmuir probe was used to observe the effect of this grid drive on the plasma.

The signal seen by the probe and the current flowing into the grid are shown in Figure (4-6). It can be seen that the

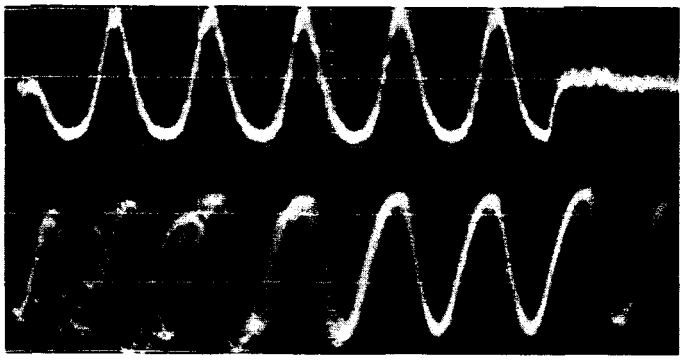

Upper Trace: Driving Current to Grid
Vertical: 20 ma/div
Horizontal: 100 μs/div

Lower Trace: Probe Current
Vertical: 10 ma/div
Horizontal: 100 μs/div

Upper and lower traces triggered simultaneously
Probe 24.5 cm. from grid
Pressure: .043 Torr.
Discharge Current: 500 ma.

Fig. 4-6. Driven Grid and Probe Signals

effect of the grid signal is to synchronize the striations in the plasma for a time duration equal to the "on" time of the modulation. The time interval between the start of the grid drive and the appearance of the signal at the probe was a direct function of the position of the probe relative to the grid. By observing the probe signal as the probe was slowly moved from the grid to the anode we ascertained that the envelope of the signal reached the probe at a later time as the probe was moved away from the grid; thus the signal was traveling from grid to anode. However, we also observed that the individual synchronized striations inside of the envelope were moving in the opposite direction, i.e., from the anode toward the cathode. Therefore this phenomenon qualitively displayed the features of a backward wave—a group velocity directed toward the anode and a phase velocity in the opposite direction.

CHAPTER V

DISCUSSION OF THE RELATION OF THE EXPERIMENTAL DATA TO THE THEORIES OF PLASMA-ACOUSTIC WAVE PROPAGATION

5.1 Introduction

The data of Chapter 4 which could be compared with that of other investigators has shown that the striations which we observed were qualitatively and quantitatively similar to striations described in other papers, with the exception of some discrepancies of questionable importance.

In this chapter we will discuss the question of a possible relationship between the propagation of the striations and plasma-acoustic waves.

The probe data of Section (4.5) indicates that the electron density varies by as much as a factor of five during the period of the striation and that the electron temperature may vary by a factor of two. Variations of this magnitude introduce nonlinear terms into the equations describing the motion of the charged particles and imply that inelastic processes are occurring which have not been included in the initial equations. Nonetheless, it is conceivable that the low frequency behavior

of our weakly ionized discharge ($\frac{N_e}{N_n} \sim 10^{-5}$) might not depart significantly from that predicted by a linear theory because of the predominance of the neutral fluid.

A direct comparison of the velocities and amplitudes given in Chapter 4 to the theoretical requirements of non-linear and linear theories of plasma-acoustic wave propagation will demonstrate that none of these theories adequately describe the propagation of the striations.

5.2 Comparison of Experimental Data with Plasma-Acoustic Wave Theory

Let us first consider the magnitudes of the striations' velocities. The highest velocities were observed at low pressures. As the pressure was increased the velocity decreased to below the adiabatic sound speed of the neutral fluid (3.23×10^4 cm.sec.$^{-1}$). This behavior was not unique to our experiment; for example, most of the velocities reported in Reference (1) at pressures of 12 torr. were below the neutral sound speed. We assume that the physical processes responsible for the propagation of the striations do not depend upon whether the velocities are super- or subsonic since the transition apparently occurs smoothly as the pressure is increased. This assumption

requires that the theoretical explanation of the striations be valid for velocities above or below the neutral sound speed.

In Chapter 2 we stated that experimental evidence (see Section 4.2) indicated a close coupling of the three kinds of particles and that this coupling justified the use of a single-fluid model for investigating non-linear behavior. In the absence of any drift velocities, all of the non-linear waves described in Chapter 2 had velocities at least as great as the local speed of sound. We also demonstrated that if the wave propagates in the direction of the ion drift, as it is observed to propagate in our experiment, then the inclusion of drift velocities in the one-fluid model can only increase the non-linear wave velocities which are observed in the stationary frame of reference. These facts lead us to the conclusion that the observation of subsonic velocities of propagation for striations which do not differ in any other way from striations with supersonic velocities is contrary to all one-fluid non-linear theories of plasma-acoustic wave propagation.

The linear multi-fluid theory is not restricted by a lower limit on the possible phase velocity. Equation (2-20) shows that a wave solution exists that gives a phase velocity

$$5\text{-}1)\quad V_{pH} = U_p\left[\frac{2\omega}{\nu_{in}}\right]^{1/2};\ \omega^2 << \nu_n(\nu_{in} + \nu_{en}\,(\frac{m_e}{m_i}))$$

This phase velocity results from finding the very low frequency and low percentage of ionization limit of

$$5\text{-}2)\quad \frac{k^2U_e^2}{\omega^2} = \frac{1 - \frac{\omega_e^2}{\omega^2} + i\,(\frac{\nu_e}{\omega} - \frac{\nu'\omega_e^2}{\omega^3})}{1 - \frac{\omega_i^2}{\omega^2} + i\,(\frac{\nu_i + \nu_n}{\omega} - \frac{\omega_i^2\nu_n}{\omega^3})};$$

therefore, it was the phase velocity and damping length predicted by this equation which we attempted to match to the experimental data. A computer program was written which, with particle densities and temperatures as input data, first calculated the values of the collision frequencies, sound speeds, and plasma frequencies, and then solved equation (5-2) for the phase velocity and damping length as evaluated functions of frequency. Expressions for classical elastic collisions were used to evaluate the collision frequencies. With the assumption that $T_e >> T_{i,n}$, the collision frequencies for unlike charged particles varies as $T_e^{-3/2}$ and the charged particle-neutral atom collision frequencies vary as $(T_{i,e})^{1/2}$.

The experimental results which most closely matched equation (5-2) came from data taken with a pressure of .043 torr. and 500 milliamperes discharge current. (Graphs of time versus distance and amplitude versus distance for this case were given in Section 4.2).

Figure (5-1) shows the measured phase velocity and phase velocities calculated from equation (5-2) as functions of frequency. The constant value given for the measured phase velocity is that which was obtained in the region toward the anode end of the positive column and thus represents a maximum value at this pressure and current (Section 4.2). Curve A is the phase velocity obtained from equation (5-2) by using the electron temperature and density, 1.86×10^4 °K and 1.3×10^{10} cm.$^{-3}$, measured with the Langmuir probe. Since the phase velocity calculated from this data was higher than the observed velocity, we set the measured value equal to $(\frac{\gamma kT_e}{m_i})^{1/2}$ and obtained the value of 6.46×10^3 °K for T_e. Inserting this value of T_e into equation (5-2) resulted in the curve labeled B in Figure (5-1). Both of the curves calculated from equation (5-2) showed a variation of phase velocity with frequency, but the experimental data indicated a constant phase velocity.

In Figure (5-2) we compare the damping length predicted by

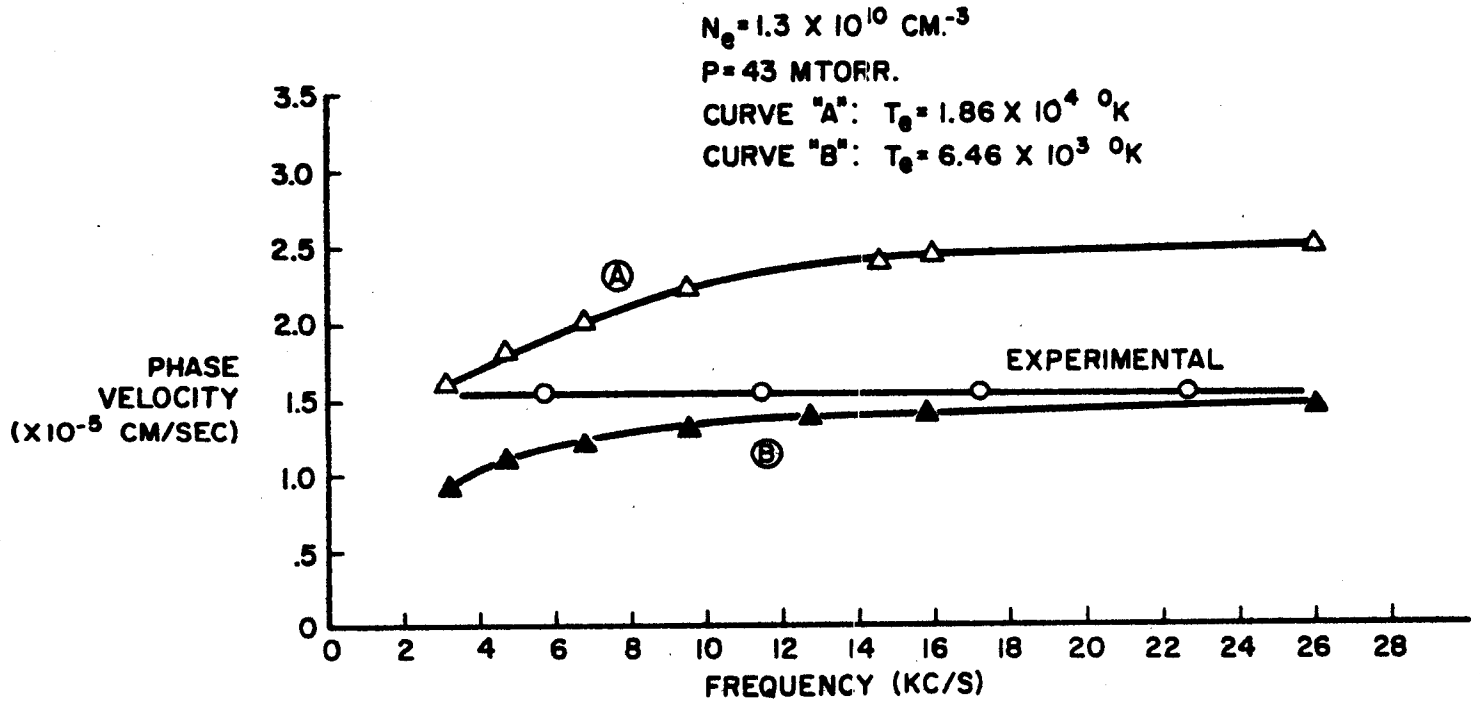

FIG. 5-1 PHASE VELOCITY VERSUS FREQUENCY.

equation (5-2) with the experimental curve. As we stated in Section 4.2, the experimental damping lengths should only be interpreted as lower limits for the actual damping length. Nevertheless, we see in Figure (5-2) that equation (5-2) predicts much heavier damping than we have observed. The predicted damping also shows very little change with frequency in the range of the experimental frequencies.

We also tried to obtain a better match between theory and experiment by adjusting the values of collision frequency and electron density. None of these attempts were successful.

We emphasize that the curves of Figures (5-1) and (5-2) represent the best match which we were able to obtain between the linear theory and the experiment. The situation progressively deteriorated as we considered data taken at higher pressures.

The discrepancies between the linear theory and the data are not resolved by a consideration of fluid drift velocities. For our experiment we expect $V_{oi} \lesssim 10^4$ cm.sec.$^{-1}$,[21] which means that the ratio $(\frac{V_{oi}}{U_p}) \lesssim .1$. Thus V_{oi} can have little effect on the observed drift velocity or attenuation, as shown by letting $\frac{V_{oi}}{U_p} \lesssim .1$ in equations (2-27a) and (2-27b).

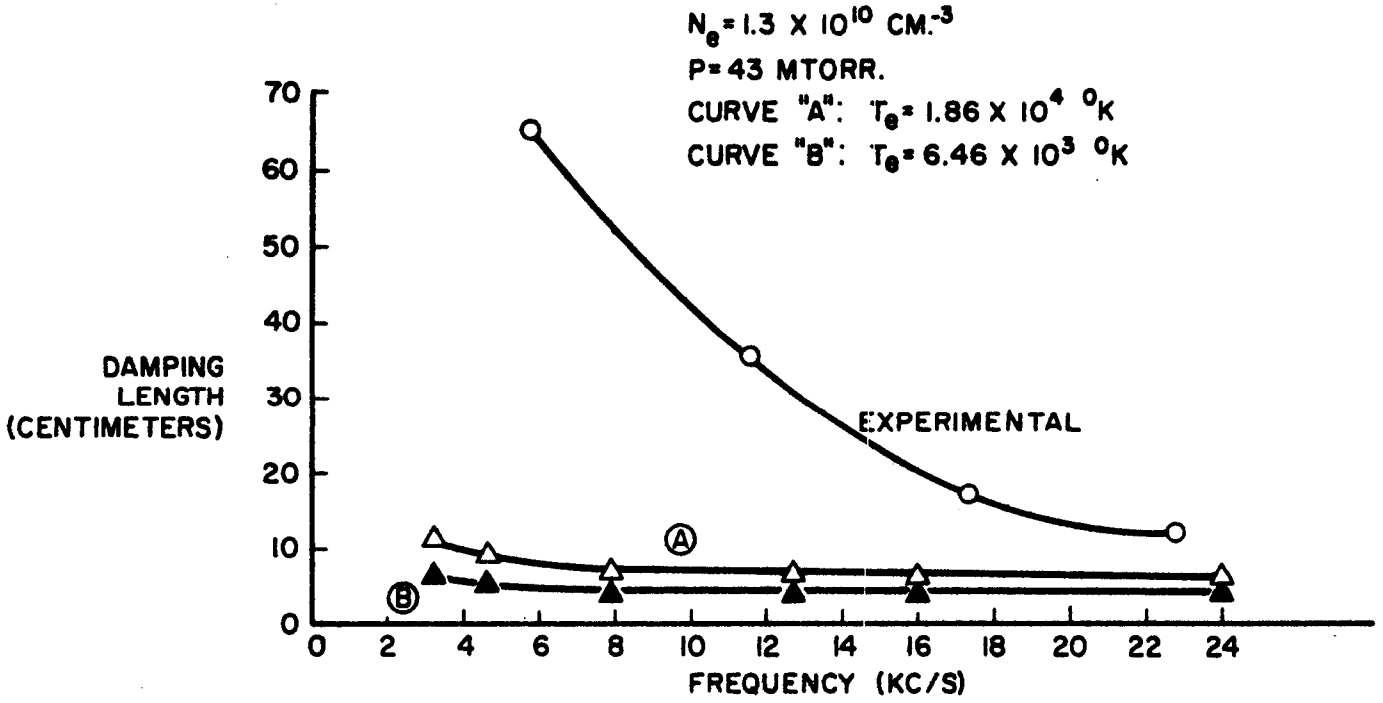

FIG. 5-2 DAMPING LENGTH VERSUS FREQUENCY.

The results of this section indicate that the movement of the striations through the positive column is not adequately explained by either a one-fluid non-linear theory nor a three-fluid linear theory of plasma-acoustic wave propagation.

CHAPTER VI

SUMMARY AND SUGGESTIONS FOR FUTURE WORK

6.1 Summary

Experiments were performed in a hot-cathode glow discharge which allowed us to determine the velocity, amplitude, fundamental frequency, and other parameters of the moving striations which occur naturally in this type of discharge. A comparison of these parameters with those given for similar experiments performed by other investigators at higher gas pressures indicated that the phenomenon we observed was not unique to the geometry or operating conditions of our discharge tube but was a result of the same physical processes operative at the higher pressures.

The low velocities of propagation of the striations at some pressures was shown to be incompatible with non-linear plasma-acoustic wave theories derived from a one-fluid model. The inclusion of drift velocities in the one-fluid model did not change this conclusion.

The solutions to our linear multi-fluid theory of longitudinal wave propagation in a partially ionized gas included

the dispersion relation for a wave which is able to propagate with a very low phase velocity. This dispersion relation was evaluated by a computer for the plasma parameters descriptive of our discharge tube.

It was not possible to find a correspondence between the computer results and our experimental results. Adjustment of the values of collision frequencies, plasma frequencies, or drift velocities was not sufficient to resolve the discrepancies.

On the basis of the failure of both the non-linear and linear theories to correspond to the observed behavior of the striations we concluded that there is no relation between the striations and plasma-acoustic wave theory, a relationship that has been suggested or assumed by various investigators since 1930.

6.2 Suggestions for Future Work

The failure of plasma-acoustic wave theories in explaining the behavior of the striations, plus the observations by Sodomsky[11] and ourselves of five hundred percent variations in the electron density, strongly indicates that the correct explanation of this phenomenon might be offered by ionization wave theories such as those of References (4) and (5). However,

given the present state of development of such theories, it is doubtful that they can be compared to experimental data in a meaningful manner.

There is at least one experiment similar to the one reported in this paper which should be performed. Disturbances with frequencies on the order of kilocycles per second and velocities of approximately 10^6 centimeters per second have been observed in the steady-state plasma beam produced by reflex-discharge plasma sources.[23] Through the use of the techniques reported in this paper and the solutions to the multi-fluid linear theory of Tanenbaum and Meskan,[19] it should be possible to determine whether that phenomenon is of the same nature as the striations in glow discharges or if they are related to plasma-acoustic waves. If they do represent plasma waves, the reflex-discharge will prove to be a most useful high-electron-temperature device for the study of wave phenomena under steady-state conditions.

APPENDIX

A.1 Dispersion Relations for Longitudinal Waves in a Partly Ionized Gas[19]

It is assumed that the following statements are valid for the plasma medium which we are considering:

1. Unbounded space.
2. No external magnetic field perpendicular to the direction of wave propagation.
3. A fixed percentage of ionization.
4. Three kinds of particles; ions, electrons, and neutral atoms.
5. Particle densities at which the continuum fluid equations are valid.

The derivation of the unsimplified dispersion equation is similar to the procedure of Tanenbaum and Mintzer.[25] Letting the subscript α denote the electron, ion, or neutral fluids, we initially write the following equations for each fluid:

A-1) Conservation of number density,

$$\frac{DN_\alpha}{Dt} + N_\alpha \nabla \cdot \vec{V}_\alpha = 0$$

A-2) Conservation of momentum,

$$\frac{D\vec{V}_\alpha}{Dt} = \frac{q_\alpha}{m_\alpha} \vec{E}_\alpha + \frac{q_\alpha}{m_\alpha} (\vec{V}_\alpha \times \vec{B}) - \frac{\nabla P_\alpha}{\rho_\alpha}$$

$$- \sum_{\beta} \nu_{\alpha\beta} (\vec{V}_\alpha - \vec{V}_\beta)$$

A-3) Conservation of energy (adiabatic energy law),

$$P_\alpha N_\alpha^{-\gamma} = \text{const.}$$

A-4) Ideal gas equation of state,

$$P_\alpha = N_\alpha k T_\alpha$$

A-5) Maxwell's equation,

$$\nabla \cdot \vec{E} = \frac{1}{\varepsilon_o} \sum_\alpha N_\alpha q_\alpha \qquad (q_n = 0)$$

where

A-6) $\rho_\alpha \equiv N_\alpha m_\alpha$

A-7) $\nu_{\alpha\beta} \equiv$ Effective collision frequency for momentum transfer.

$$\rho_\alpha \nu_{\alpha\beta} = \rho_\beta \nu_{\beta\alpha} \; ; \qquad \alpha \neq \beta \; .$$

We next assume that a plane wave solution exists and that the variables are given by

A-8) $N_\alpha = N_{o\alpha} + n_\alpha e^{i(kx - \omega t)}$

$$\vec{V}_\alpha = \vec{V}_{o\alpha} + \vec{v}_\alpha e^{i(kx - \omega t)}$$

$$P_\alpha = P_{o\alpha} + P_\alpha e^{i(kx - \omega t)}$$

$$\vec{E}_\alpha = \vec{E}_\alpha e^{i(kx - \omega t)}$$

$$\vec{B}_\alpha = \vec{B}_\alpha e^{i(kx - \omega t)}.$$

These variables are inserted into equations (A-1) through (A-5), and the resulting set of equations is solved for $\vec{V}_\alpha$ and linearized. The linearization is achieved by discarding all non-linear space and time dependent terms.

The resulting linearized set of equations can be written, in matrix notation,

$$\text{A-9)} \quad \overline{\overline{A}} \cdot \vec{V}_\alpha = 0$$

where $\overline{\overline{A}}$ is a three-by-three matrix and $\vec{V}_\alpha$ is a column, or vector, matrix. The existence of non-trivial solutions for $\vec{V}_\alpha$ requires that the determinant of the coefficient matrix $\overline{\overline{A}}$ be equal to zero;

$$\text{A-10)} \quad \det \overline{\overline{A}} = 0.$$

Condition (A-10) gives an algebraic equation of the form

$$\text{A-11)} \quad A(\omega)k^6 + B(\omega)k^4 + C(\omega)k^2 + D(\omega) = 0$$

in which the coefficients A, B, C, and D are complicated functions of frequency, collision frequencies, plasma frequencies, and sound speeds.

Tanenbaum and Mintzer dealt with equation (A-11) by seeking solutions for k^2 which were approximately valid for particular ranges of ω. Moreover their analysis assumes approximately equal temperatures for all constituents.

We use a different kind of approximation to find solutions of equation (A-11) which are valid over a wide range of frequencies. Many plasmas produced in the laboratory have variables which lie within the ranges

A-12) $10^{10} < N_n < 10^{16}\ cm.^{-3}$; $10^9 < N_{i,e} < 10^{14}\ cm.^{-3}$

$T_e >> T_{i,n}$; $T_{i,n} < 10^4\ ^oK < T_e$.

Using these inequalities we find that the following inequalities are valid:

A-13) $U_e^2 >> U_p^2 >> U_{i,n}^2$

$(\nu_i + \nu_n) << \nu_e$

$$\nu_e(\nu_i + \nu_n) << \omega_e^2$$

$$\nu_e U_i^2 << \nu_i U_e^2$$

$$\nu_i \nu_n << \omega_i^2 \ .$$

The terms in (A-13) are defined by

A-14) $$\nu_\alpha \equiv \nu_{\alpha\beta} + \nu_{\alpha\delta}; \qquad \alpha \neq \beta, \delta \ ; \quad \beta \neq \delta$$

$$U_\alpha^2 = \frac{\gamma k T_\alpha}{m_\alpha} \quad ; \qquad U_p^2 = \frac{\gamma k T_e}{m_i} \qquad (T_e >> T_i) \ .$$

In order to determine the inequalities (A-13) we use the following expressions for the collision frequencies for momentum transfer[26] (we assumed $T_i \triangleq T_n$, $m_n = m_i$):

A-15) $$\nu_{in} = \frac{1}{2} \left(\frac{3kT_n}{m_n}\right)^{1/2} \pi(2r_n)^2 \, Nn$$

$$\nu_{en} = \pi r_n^2 \, Nn \left[\frac{3kT_e}{m_e}\right]^{1/2}$$

$$\nu_{ni} = \frac{1}{2} \left(\frac{3kT_n}{m_n}\right)^{1/2} \pi(2r_n)^2 N_i$$

$$\nu_{ne} = \nu_{en} \left[\frac{m_e N_e}{m_n N_n}\right]$$

$$\nu_{ie} = \frac{m_e}{m_i} (6.1 \times 10^{-3})\left(\frac{T_e}{300}\right)^{-3/2} N_e$$

$$\nu_{ei} = \nu_{ie}\left(\frac{m_i N_i}{m_e N_e}\right) .$$

These collision frequencies are related to the actual number of collisions per unit time, $\nu'_{\alpha\beta}$, by

$$\text{A-16)} \quad \nu_{\alpha\beta} = \frac{m_\beta \nu'_{\alpha\beta}}{m_\alpha + m_\beta} .$$

Using the inequalities (A-13) reduced the coefficients in equation (A-11) to

$$\text{A-17)} \quad A(\omega) \triangleq U_e^2 U_i^2 U_n^2$$

$$B(\omega) \triangleq - U_e^2\{U_i^2(\omega^2 + i\omega\nu_n) + U_n^2(\omega^2 - \omega_i^2 + i\omega\nu_i)\}$$

$$C(\omega) \triangleq U_e^2\{\omega^4 - \omega^2(\omega_i^2 - i\omega(\nu_i + \nu_n))$$

$$- i\omega_i^2\omega\nu_n(1 + \frac{\rho_n U_n^2}{\rho_i U_p^2})\}$$

$$D(\omega) \triangleq - [\omega^6 - \omega^4(\omega_e^2 - i\omega\nu_e) - i\omega^3\omega_e^2\nu_n \frac{\rho_n}{\rho_i}] .$$

The only term which causes any difficulty is the factor

$$\left[1 + \frac{\rho_n U_n}{\rho_i U_p}\right] \text{in } C(\omega).$$

For a gas which is ionized sufficiently so that

A-18) $\rho_n U_n^2 << \rho_i U_p^2$, $(N_n T_n << N_e T_e)$

we find the three roots to equation (A-11)

A-19) $k^2U_i^2 = \omega^2 - \omega_i^2 + i\omega\nu_i$

A-20) $k^2U_n^2 = \omega^2 + i\omega\nu_n$

$$\text{A-21)}\quad \frac{k^2U_e^2}{\omega^2} = \frac{1 - \frac{\omega_e^2}{\omega^2} + i\left(\frac{\nu_e}{\omega} - \frac{\nu'\omega_e^2}{\omega^3}\right)}{1 - \frac{\omega_i^2}{\omega^2} + i\left(\frac{\nu_i + \nu_n}{\omega} - \frac{\omega_i^2\,\nu_n}{\omega^3}\right)}$$

$$\nu' = \nu_n + \nu_{in} + \nu_{en}\left(\frac{m_e}{m_i}\right).$$

Equations (A-19) through (A-21) are valid solutions to equation (A-11) except for $\omega \triangleq \omega_i$. (For $\omega = \omega_i$ we use a separate analysis, which begins with the unsimplified equation (A-11), and find no resonances at ω_i). Physically, we expect that the upper frequency limits for the validity of solutions (A-19) through (A-21) will be those frequencies for which the initial continuum equations, (A-1) through (A-4), are no longer valid.

For the case of a weakly ionized gas where

$$\text{A-22)}\quad N_nT_n \gtrsim N_eT_e$$

we find that the term $\frac{\rho_n U_n^2}{\rho_i U_p^2}$ does not affect the validity of solutions (A-19) through (A-21) provided

$$\text{A-23)} \quad \omega^2 \gtrsim \nu_n(\nu_{in} + \nu_{en}(\frac{m_e}{m_i})) \ .$$

(For densities and temperatures typical of our experiment, we found that $\nu_n^{1/2}(\nu_{in} + \nu_{en}(\frac{m_e}{m_i}))^{1/2}$ was often on the order of a few hundred cycles per second).

If inequality (A-23) is not satisfied, one must use other methods to determine the correct roots of equation (A-11). The three roots which are approximately correct for $\omega \to 0$ are found to be

$$\text{A-24)} \quad k^2U_T^2 \doteq \omega^2[1 + \frac{i\omega[U_T^2 - U_n^2]}{\rho \frac{\nu_n}{\rho_n} U_T^4}]$$

$$U_T^2 \equiv \sum_\alpha \frac{\gamma_\alpha P_\alpha}{\rho_\alpha}$$

$$\text{A-25)} \quad k^2 = i \frac{\omega\nu' U_T^2}{U_p^2 U_n^2}$$

A-26) $$k^2 = \frac{-\omega_p^2 U_p^2}{U_e^2 U_i^2} \; ; \qquad \omega_p^2 = \omega_e^2 + \omega_i^2$$

Equation (A-24) represents an acoustic wave for which the ions, electrons, and neutral fluids are tightly coupled.

A heavily damped ion wave is described by equation (A-26).

Equation (A-25) has two possible limits. For $\rho_n U_n^2 << \rho_p U_p^2$, $(\rho_p = \rho_e + \rho_i)$, we find

A-27a) $$k^2 U_n^2 \triangleq i \omega \nu_n$$

which is a heavily damped neutral wave.

If $\rho_n U_n^2 >> \rho_p U_p^2$, we obtain

A-27b) $$k^2 U_p^2 \triangleq i \omega (\nu_{in} + \nu_{en}(\frac{m_e}{m_i}))$$

which is the expression found by Hatta and Sato.[18]

LIST OF REFERENCES

1. T. Donahue and G. Dieke, Phys. Rev. 81, 248 (1951).

2. R. Fowler, Nature 196, 976 (1962).

3. L. Loeb, Basic Processes of Gaseous Electronics (Univ. of Calif. Press, Berkeley, Calif., 1960).

4. H. Robertson, Phys. Rev. 105, 368 (1957).

5. N. Oleson and S. Watanabe, Phys. Rev. 99, 1701 (1955).

6. L. Pekarek, Czech. Journ. Phys. B11, 729 (1961), B12 450 (1962), B13 881 (1963).

7. K. G. Emeleus, E. B. Armstrong, and T. R. Neill, Proc. Roy. Irish Acad. A54, 291 (1951).

8. G. D. Morgan, Nature 172, 542 (1953).

9. A. Cooper, J. Coulter, and K. Emeleus, Nature 181, 1326 (1958).

10. J. Coulter, Jour. Elect. Control 9, 41 (1960).

11. K. Sodomsky, Jour. Appl. Phys. 34, 1860 (1963).

12. G. Francis, Handbuch der Physik V. 22 (Springer, Berlin).

13. K. Emeleus, Advances in Electronics and Electron Physics V. 20 (Academic Press, N.Y., 1964).

14. I. Langmuir and L. Tonks, Phys. Rev. 33, (1929).

15. L. Landau and E. Lifshitz, Fluid Mechanics (Pergammon Press, London, 1959).

16. P. Little and H. Jones, Proc. Phys. Soc. London 85, 516 (1965).

17. I. Alexeff and R. V. Neidigh, Phys. Rev. 129, 516 (1963).

18. Y. Hatta and N. Sato, Proc. 5th Inter. Conf. on Ioniz. Phen. in Gases V. 1 (North Holland, Amsterdam, 1962).

19. B. S. Tanenbaum and D. A. Meskan, 6th Annual Meeting A.P.S. Div. of Plasma Physics, Nov. 1964, N.Y.

20. I. Langmuir and H. Mott-Smith, Phys. Rev. 28, (1926).

21. D. Samaras, Theory of Ion Flow Dynamics (Prentice-Hall, Englewood, N.J., 1962).

22. R. Whiddington, Nature 116, 506 (1925).

23. D. Meskan, Characteristics of a Magnetically Confined Steady State Plasma Beam, Case Institute of Technology, Plasma Research Technical Report A-20, (1963).

24. B. S. Tanenbaum, Private Communication.

25. B. S. Tanenbaum and D. Mintzer, Phys. Fld. 5, 1226 (1962).

26. T. G. Cowling, Proc. Roy. Soc. (London), A183, 453 (1945).

27. F. Crawford and S. Self, Proc. 6th Int. Conf. Ioniz. Phen., Paris V 3 (Orsay: Faculte des Sciences) 129.